Numerical simulations of *i*-process nucleosynthesis in stars constrained by nuclear physics experiments and astrophysical observations

Pavel Denissenkov

in collaboration with

Falk Herwig, Georgios Perdikakis, Marco Pignatari, Hendrik Schatz,
Artemis Spyrou, Paul Woodward,

and CaNPAN students

Lauren Harewood, Joshua Issa, Mallory Loria, and Parth Vats

Outline

1. What is *i* process and how does it differ from the *s* and *r* processes?
2. Multi-zone and one-zone models of *i*-process nucleosynthesis.
3. What are CEMP stars and their *s*, *r*, and *s/r* sub-classes?
4. Direct and indirect signatures of *i*-process nucleosynthesis in stars.
5. On the important role of the split of a He-shell flash convection zone in limiting the *i*-process neutron exposure time.
6. Comparison of results obtained with one- and multi-zone models.
7. A conclusion that some of the CEMP-*s* stars may actually be the CEMP-*i* stars.
8. MC simulations with one- and multi-zone *i*-process models for n-capture reaction rate uncertainty studies of unstable isotopes.
9. Comparison of *i*-process simulations with multi-zone RAWD and AGB models.
10. CaNPAN computational tools and related experiments.
11. Conclusions

Slow (*s*-), rapid (*r*-), and intermediate (*i*-) neutron-capture processes

Characteristic neutron densities:

$N_{n,s} \lesssim 10^{12}\ \mathrm{cm}^{-3}$,
$N_{n,r} \gtrsim 10^{20}\ \mathrm{cm}^{-3}$,

$10^{12} \lesssim N_{n,i} \lesssim 10^{16}\ \mathrm{cm}^{-3}$

Figure from Lugaro, M. et al., 2023, Annual Review of Nuclear and Particle Science, 73, 315

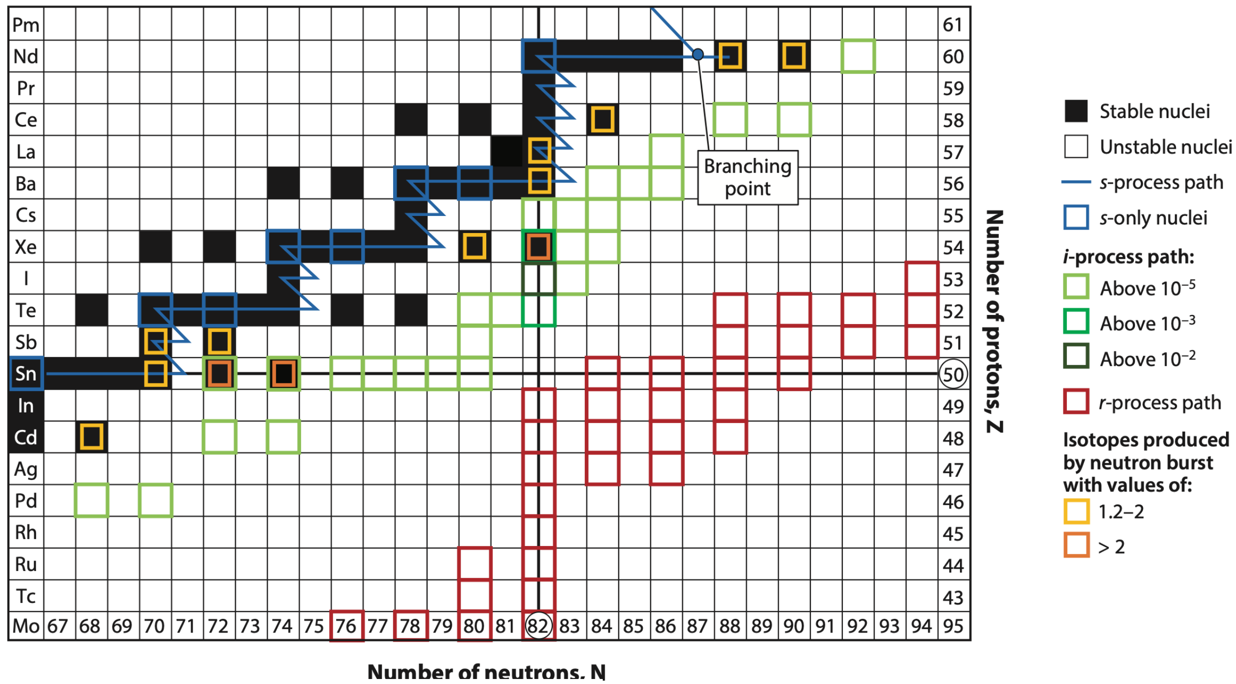

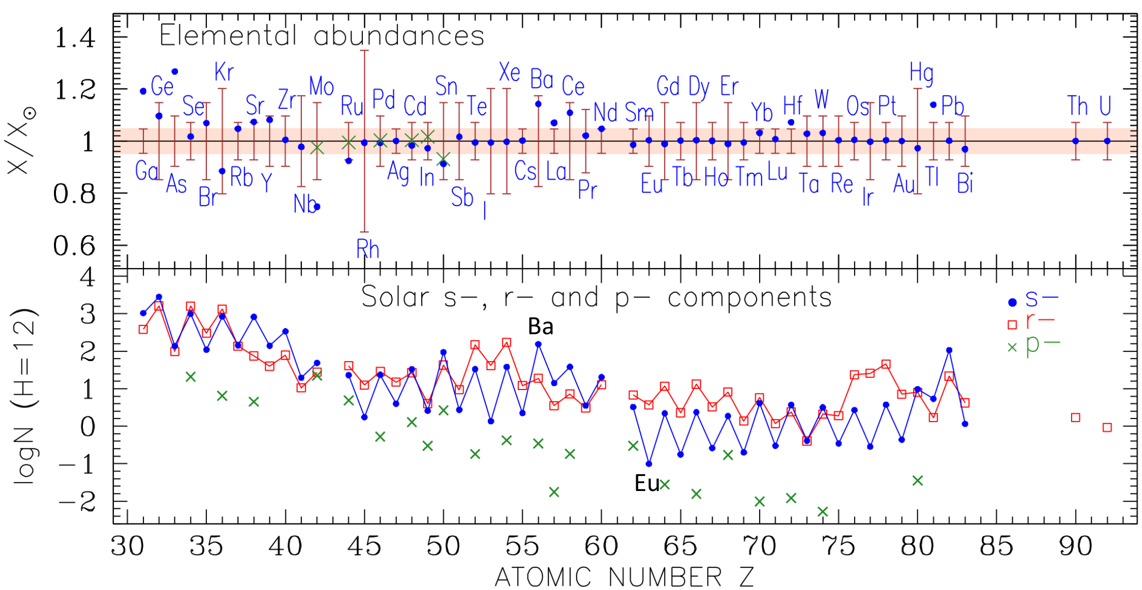

Figure from Prantzos, N. et al., 2020, MNRAS, 491, 832

Multi-zone and one-zone models of *i*-process nucleosynthesis in stars

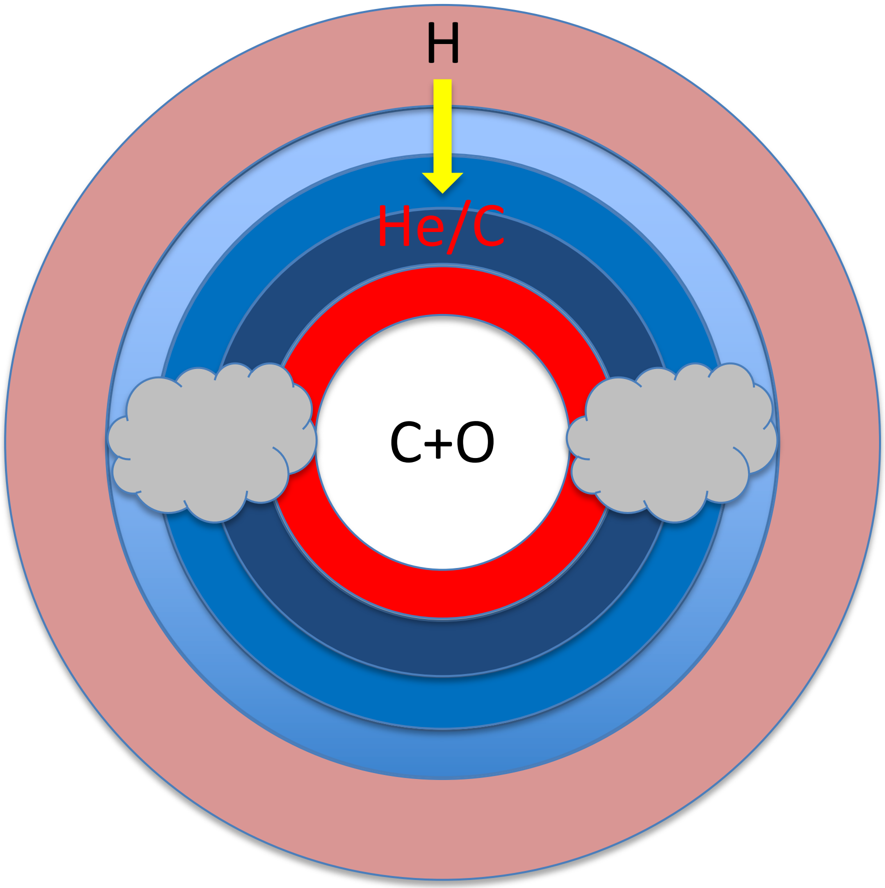

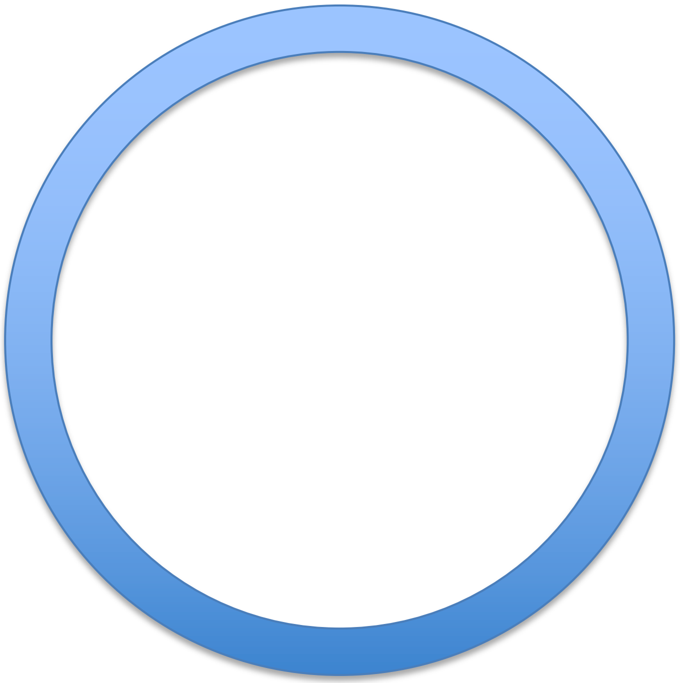

Multi-zone model: temperature (T) and density (ρ) are both increasing with depth. Convection driven by a He-shell flash ingests H into He- and C-rich zones, in which the reactions $^{12}C(p,\gamma)^{13}N(e^+ \nu)^{13}C(\alpha,n)^{16}O$ release neutrons. Therefore, the neutron density N_n is also increasing with depth.

One-zone model: T, ρ, and N_n are all constant in the zone.

Pollution of CEMP-*r/s* (CEMP-*i*) stars by products of *i*-process nucleosynthesis?

TABLE 2 Definition of subclasses of metal-poor stars

Neutron-capture-rich stars	
r-I	$0.3 \leq$ [Eu/Fe] $\leq +1.0$ and [Ba/Eu] < 0
r-II	[Eu/Fe] $> +1.0$ and [Ba/Eu] < 0
s	[Ba/Fe] $> +1.0$ and [Ba/Eu] $> +0.5$
r/s	$0.0 <$ [Ba/Eu] $< +0.5$
Carbon-enhanced metal-poor stars	
CEMP	[C/Fe] $> +1.0$
CEMP-r	[C/Fe] $> +1.0$ and [Eu/Fe] $> +1.0$
CEMP-s	[C/Fe] $> +1.0$, [Ba/Fe] $> +1.0$, and [Ba/Eu] $> +0.5$
CEMP-r/s	[C/Fe] $> +1.0$ and $0.0 <$ [Ba/Eu] $< +0.5$
CEMP-no	[C/Fe] $> +1.0$ and [Ba/Fe] < 0

[A/B] = $log_{10}\,[X(\mathrm{A})/X(\mathrm{B})]$ - $log_{10}\,[X_{\odot}(\mathrm{A})/X_{\odot}(\mathrm{B})]$, where X(A) is the mass fraction of A

Beers, T.C., Christlieb, N., 2005, ARA&A, 43,531

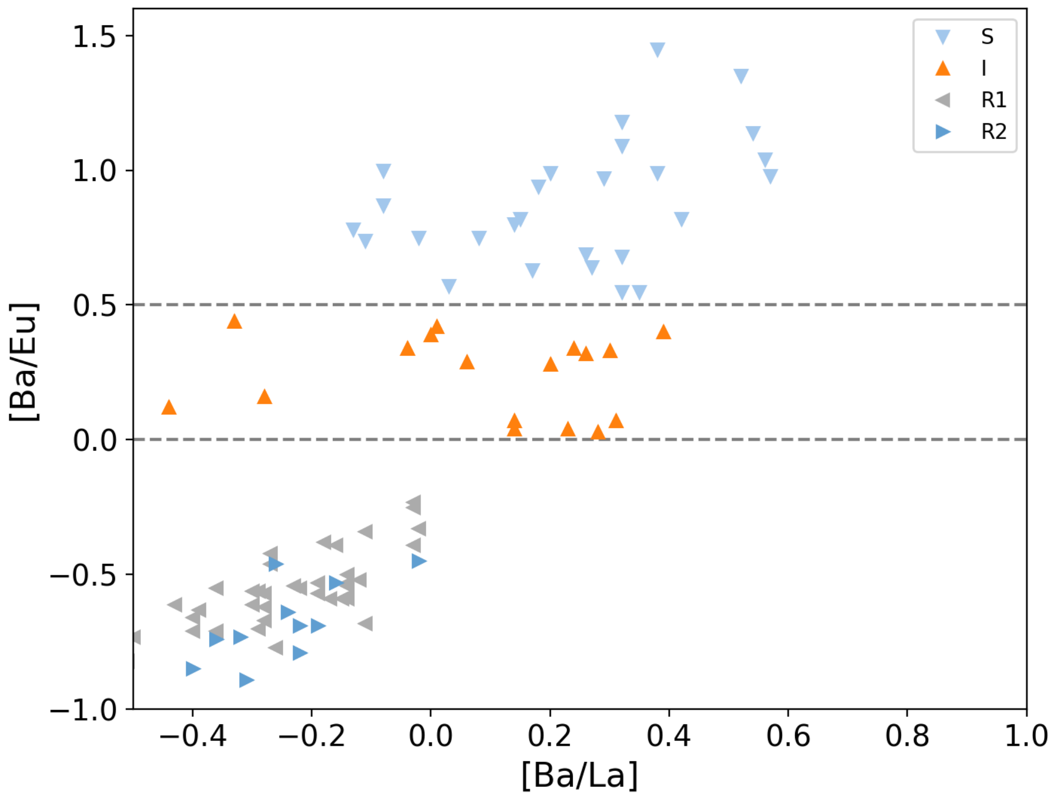

JINAbase
(https://jinabase.pythonanywhere.com)
Abohalima, A., Frebel, A., 2018, ApJS, 238, 36

CEMP stars and equilibrium *i*-process abundances from the one-zone model

TABLE 2 Definition of subclasses of metal-poor stars

Neutron-capture-rich stars	
r-I	$0.3 \leq$ [Eu/Fe] $\leq +1.0$ and [Ba/Eu] < 0
r-II	[Eu/Fe] $> +1.0$ and [Ba/Eu] < 0
s	[Ba/Fe] $> +1.0$ and [Ba/Eu] $> +0.5$
r/s	$0.0 <$ [Ba/Eu] $< +0.5$
Carbon-enhanced metal-poor stars	
CEMP	[C/Fe] $> +1.0$
CEMP-r	[C/Fe] $> +1.0$ and [Eu/Fe] $> +1.0$
CEMP-s	[C/Fe] $> +1.0$, [Ba/Fe] $> +1.0$, and [Ba/Eu] $> +0.5$
CEMP-r/s	[C/Fe] $> +1.0$ and $0.0 <$ [Ba/Eu] $< +0.5$
CEMP-no	[C/Fe] $> +1.0$ and [Ba/Fe] < 0

Beers, T.C., Christlieb, N., 2005, ARA&A, 43,531

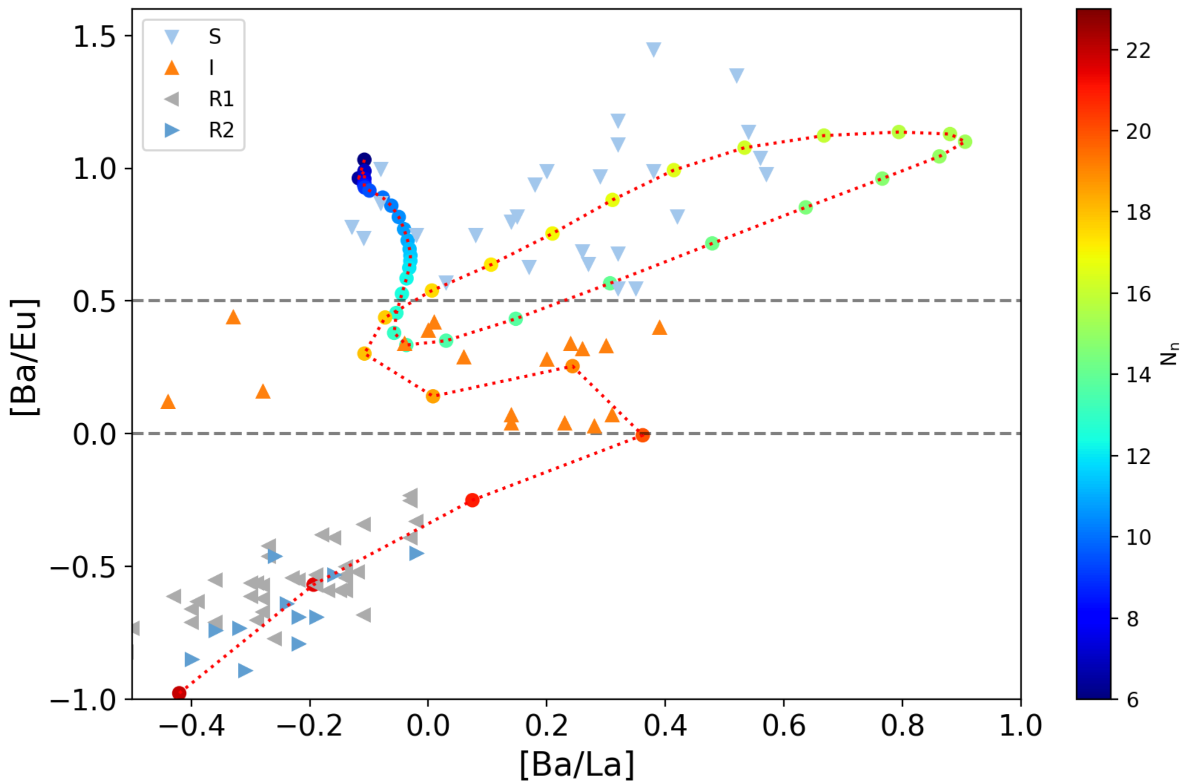

JINAbase

(https://jinabase.pythonanywhere.com)

Abohalima, A., Frebel, A., 2018, ApJS, 238, 36

One-zone computations of *i*-process nucleosynthesis: equilibrium abundances at the neutron exposure $\tau = \int_0^t N_{\mathrm{n}} v_{\mathrm{n,th}} dt \gg 1$

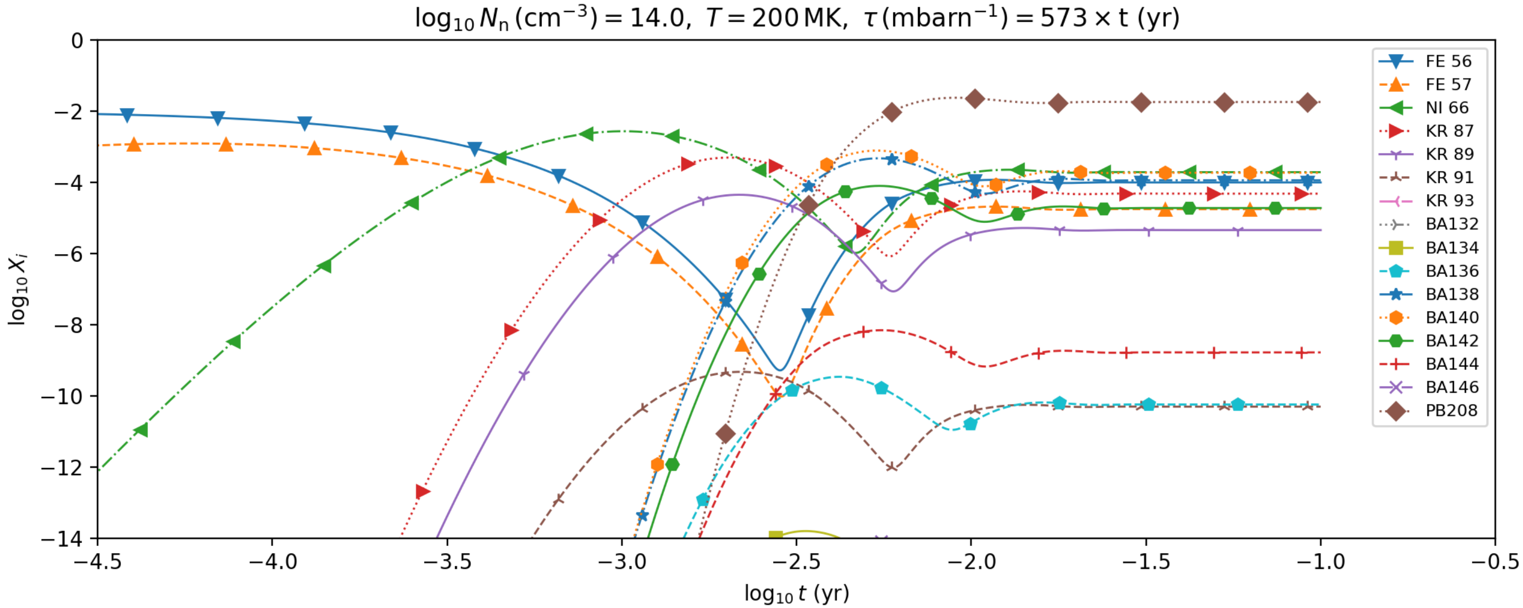

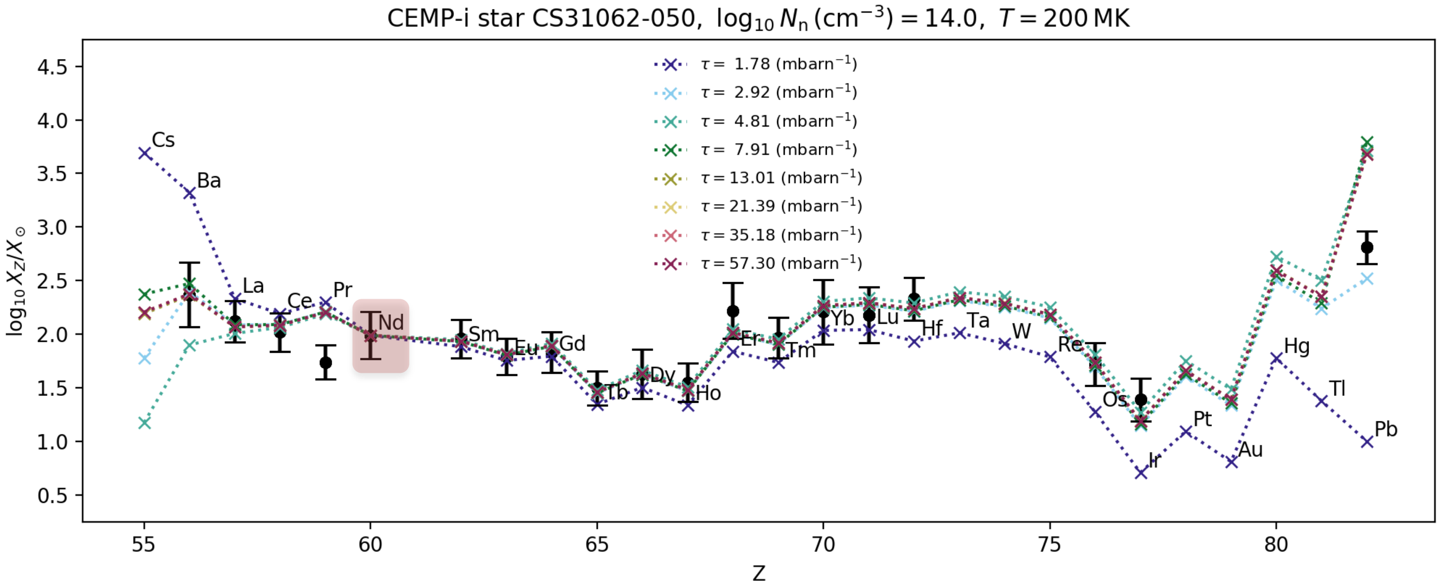

Nd is used as a pin

First, Dardelet, L. et al., (2014nic..confE.145D), and then Hampel, M., et al. (2019, ApJ, 887, 11) estimated $10^{11} \leq N_{\mathrm{n}}(\mathrm{cm}^{-3}) \leq 10^{14}$ and $1.1 \leq \tau\,(\mathrm{mbarn}^{-1}) \leq 23.2$ for 24 CEMP-*r/s* stars, with $N_{\mathrm{n}}=10^{14}\ \mathrm{cm}^{-3}$ and $\tau=3.4\ \mathrm{mbarn}^{-1}$ for CS31062-050

Indeed, some of the CEMP-*r/s* stars are probably CEMP-*i* stars

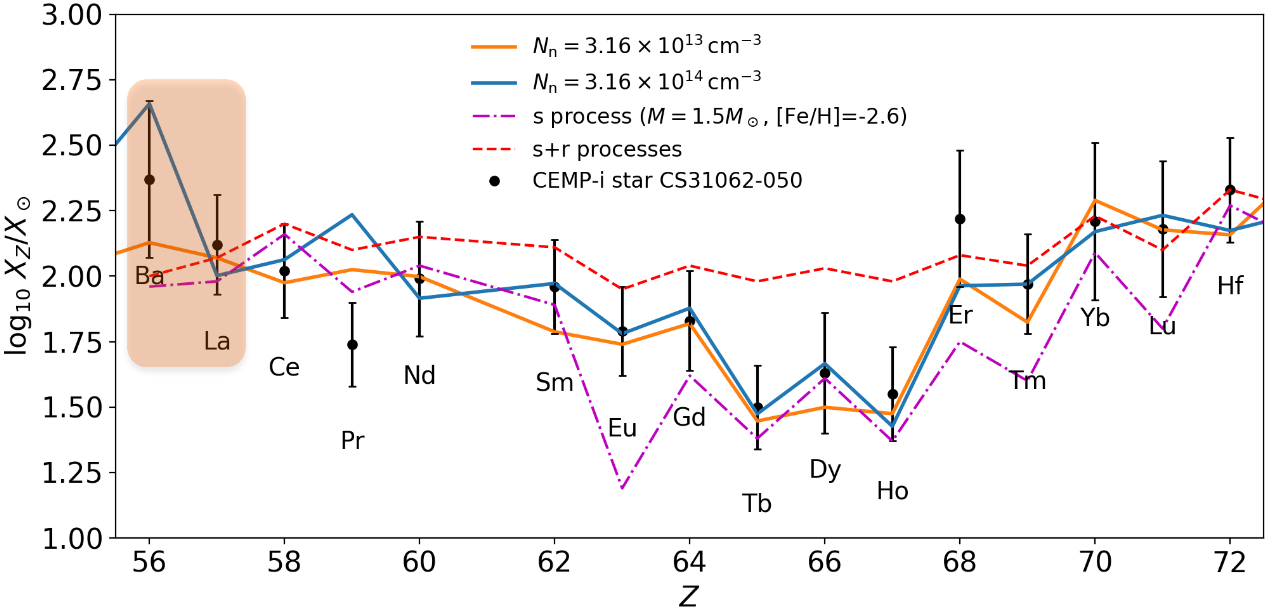

Johnson, J., A., Bolte, M., 2004, ApJ, 605,462

Lai, D.K., et al.. 2007, ApJ, 667, 1185

Bisterzo, S., et al., 2011, MNRAS, 418, 284

Note: [Ba/La] is sensitive to the value of N_n for the *i*-process equilibrium abundances calculated for constant values of N_n!

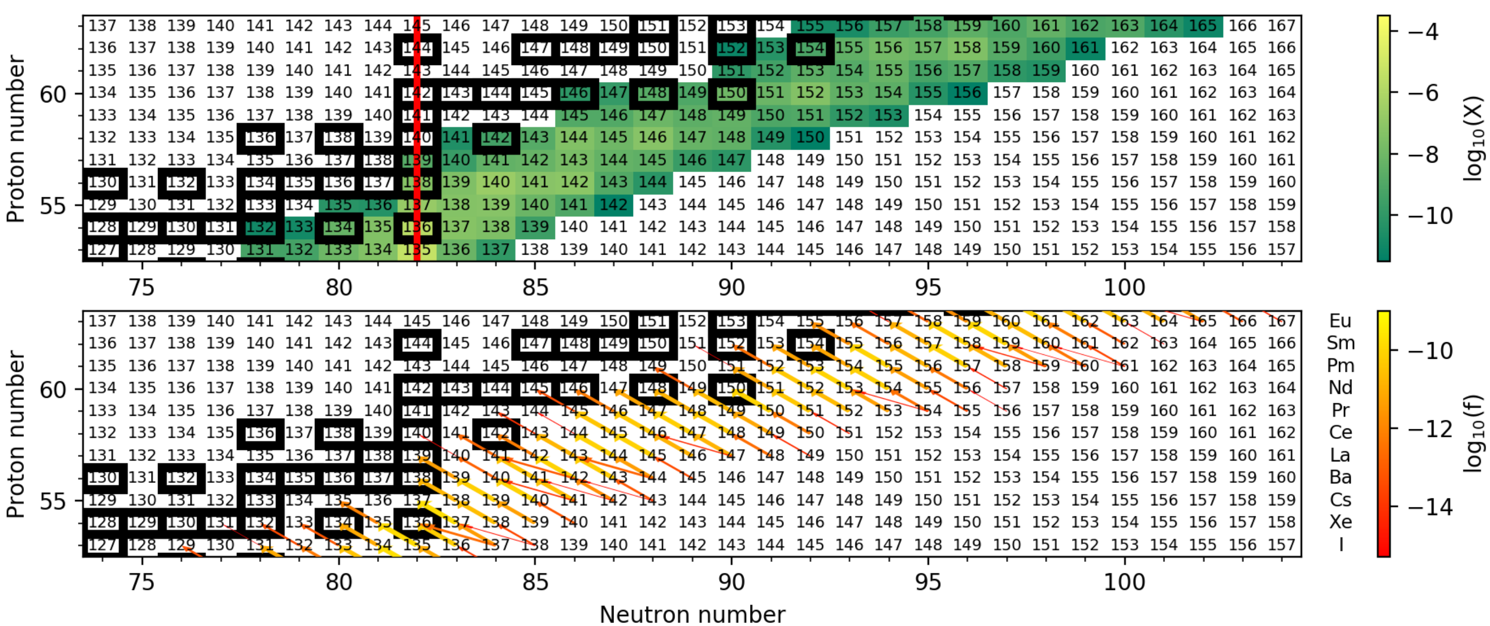

i-process path at N_n=3.16×10^{14} cm^{-3}

Multi-zone *i*-process models: He-shell flashes in the post-AGB Sakurai's object, rapidly-accreting white dwarfs (RAWDs), and low-mass metal-poor AGB stars

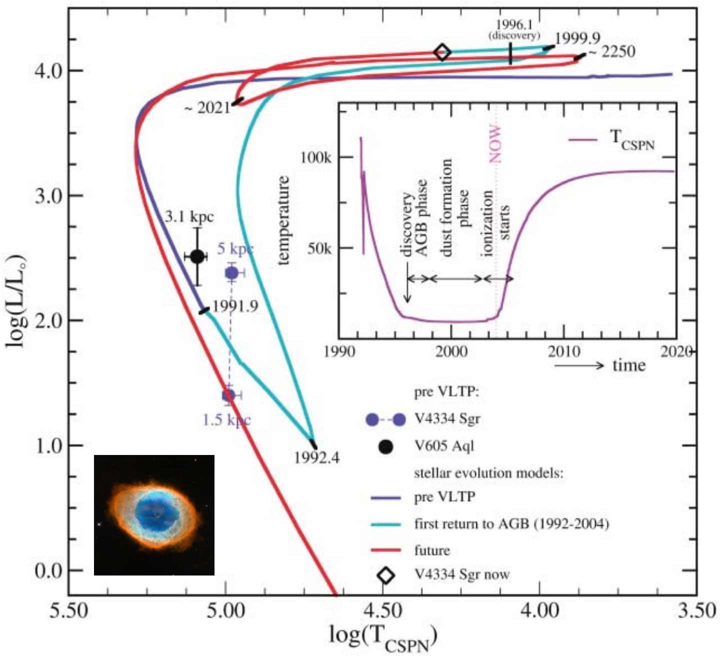

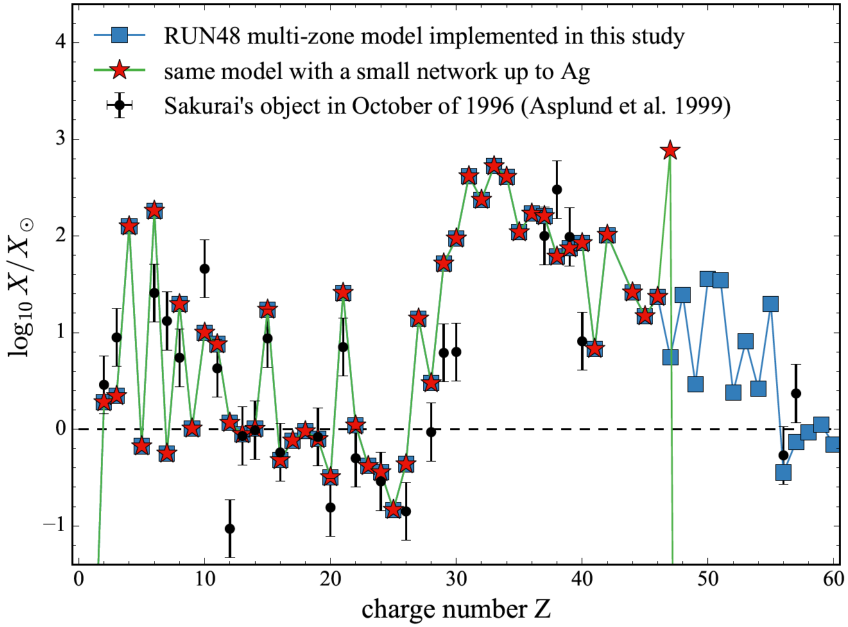

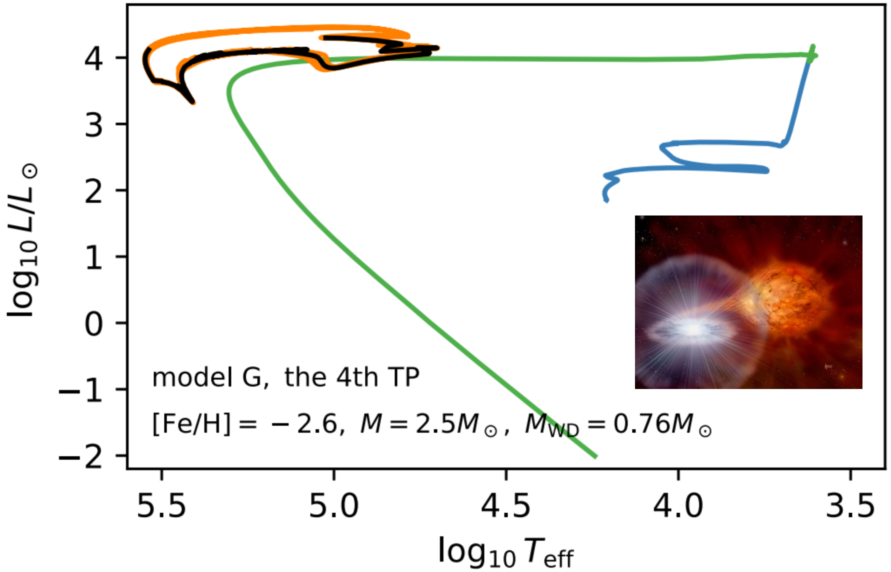

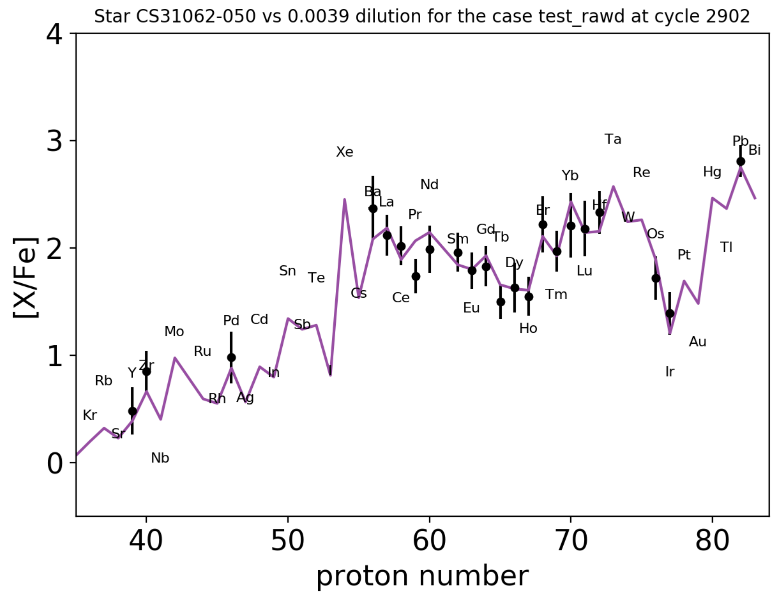

Multi-zone *i*-process models: He-shell flashes in the post-AGB Sakurai's object, rapidly-accreting white dwarfs (RAWDs), and low-mass metal-poor AGB stars

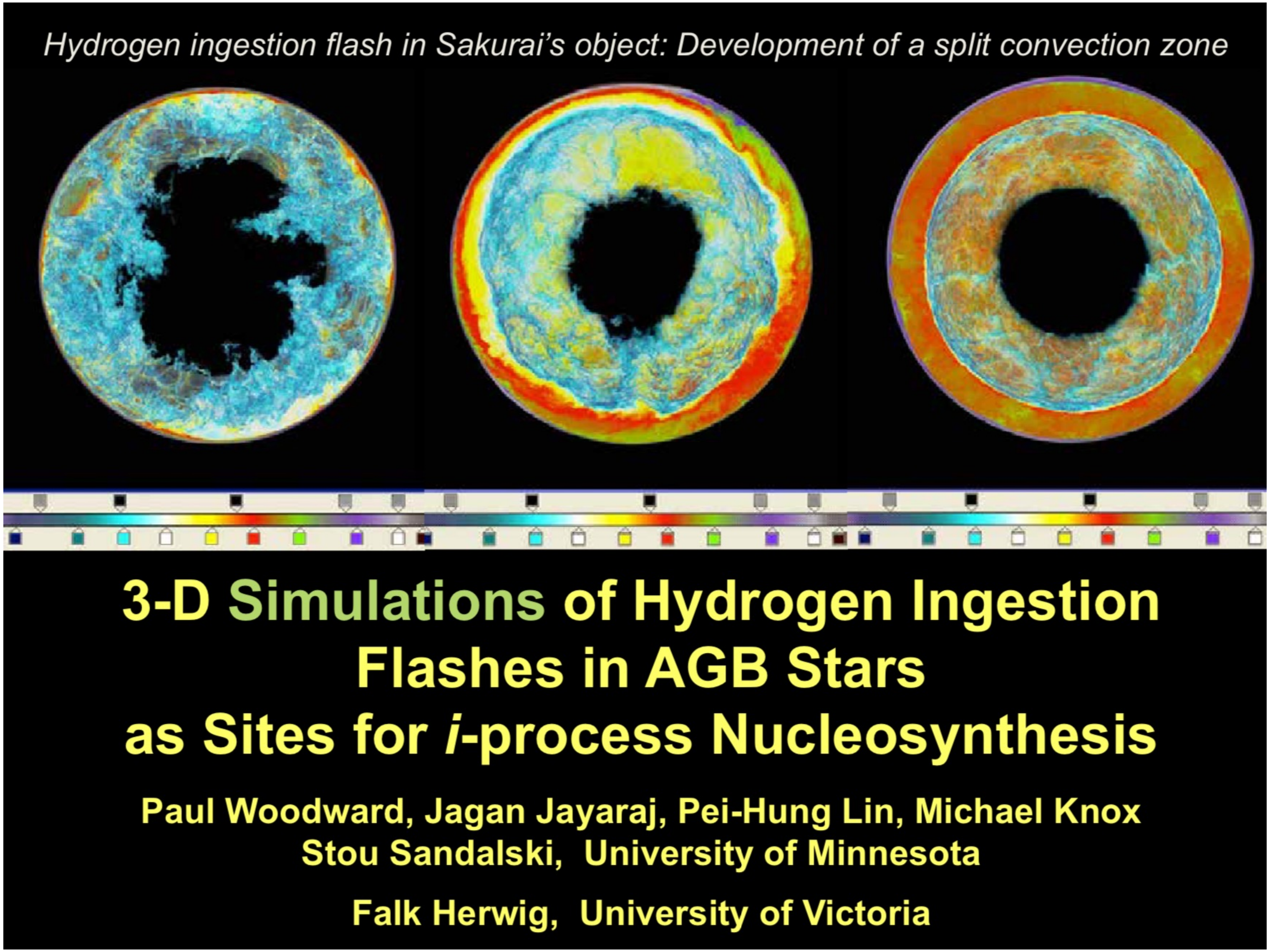

From Blue Waters User Portal

Comparison of one-zone and multi-zone RAWD and AGB models

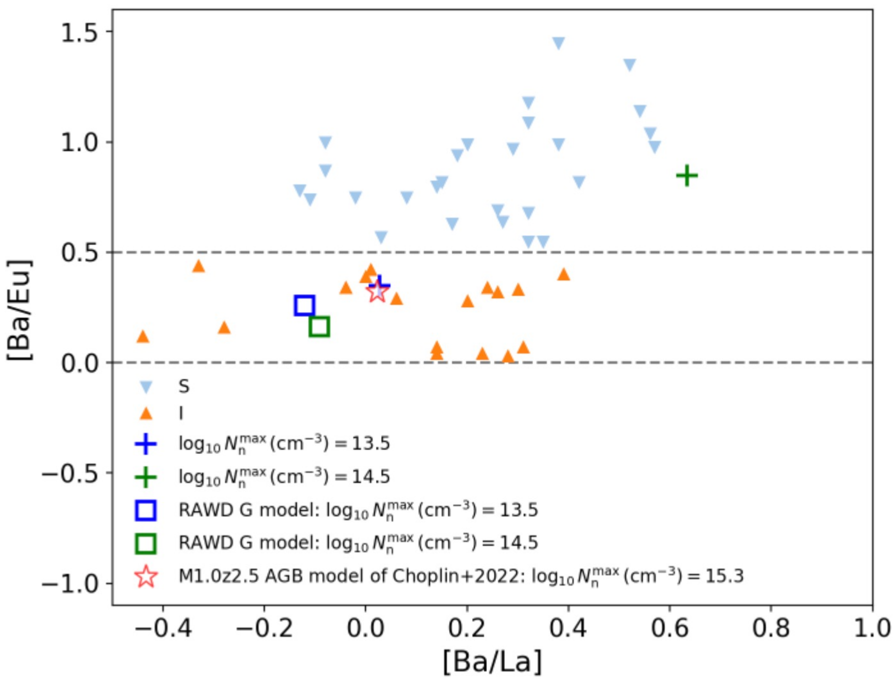

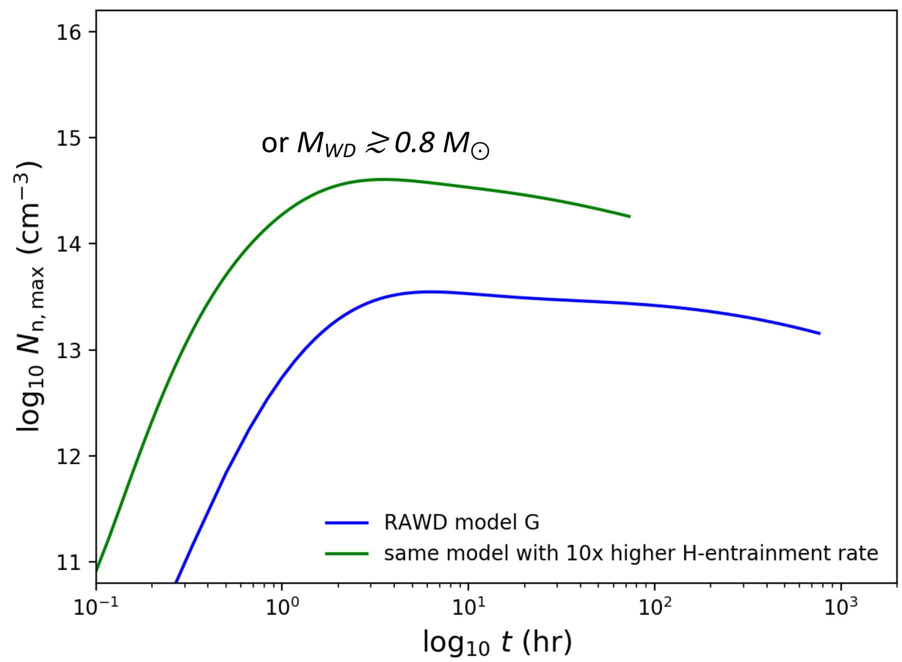

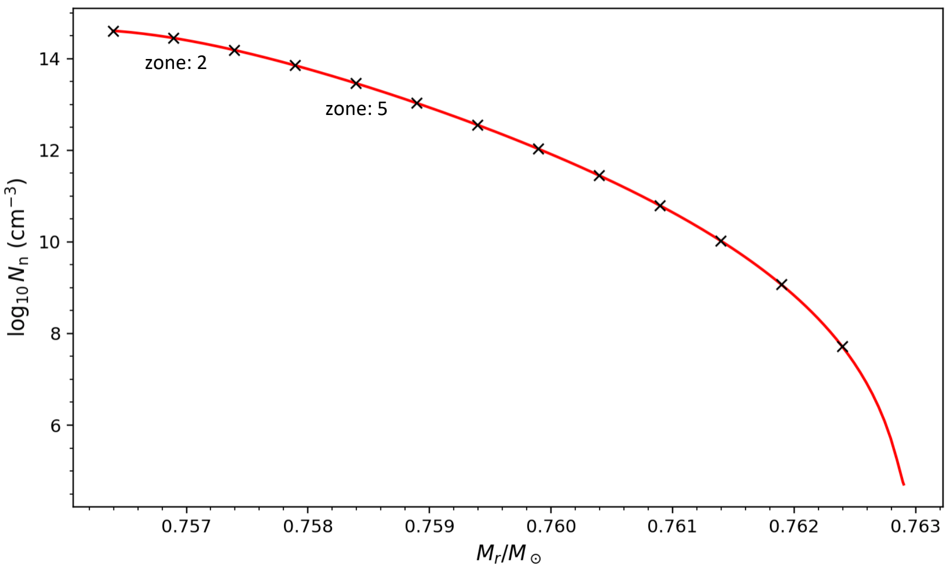

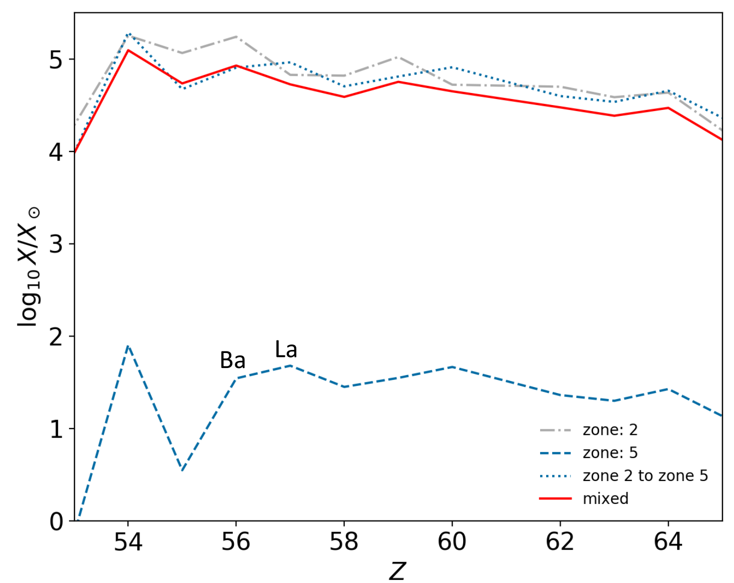

Some of the CEMP-*s* stars may actually be the CEMP-*i* stars: one-zone models

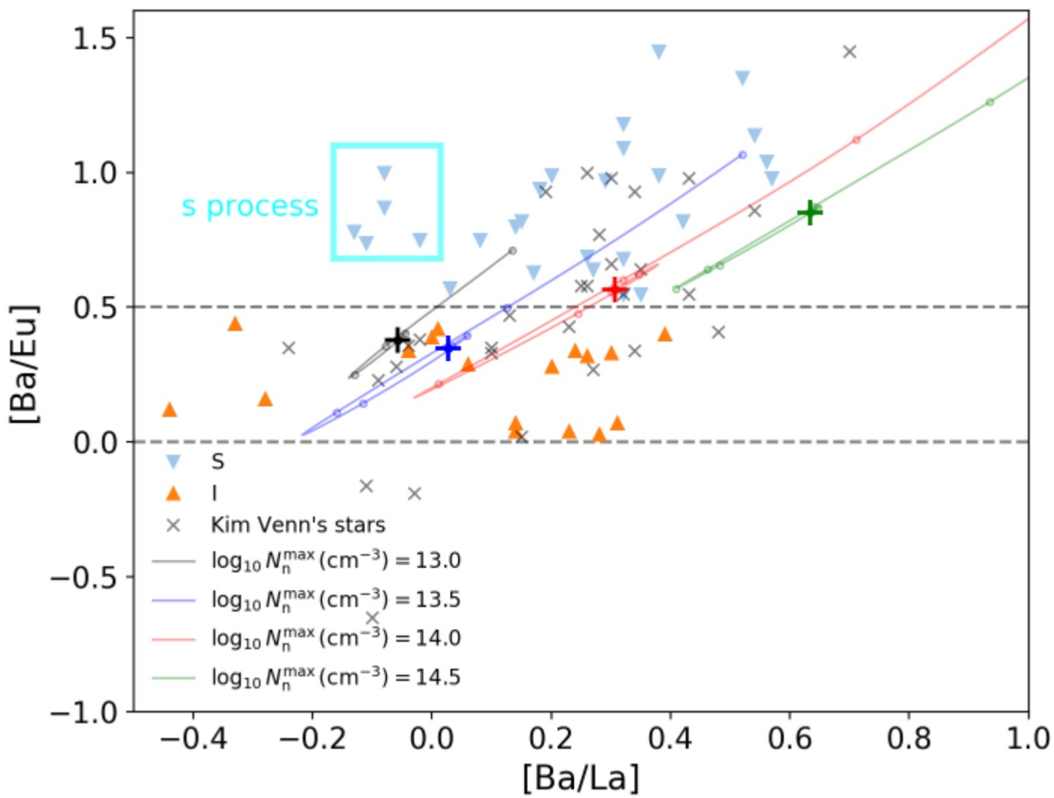

(n,γ) reaction rate uncertainties and a possibility that in some of the CEMP-*i* stars the [Ba/La] ratio has not reached its equilibrium value (curves have τ > 1.5 mbarn^{-1}) have to be taken into account

Note: [Ba/La] is sensitive to the value of N_n for the *i*-process equilibrium abundances calculated for constant values of N_n!

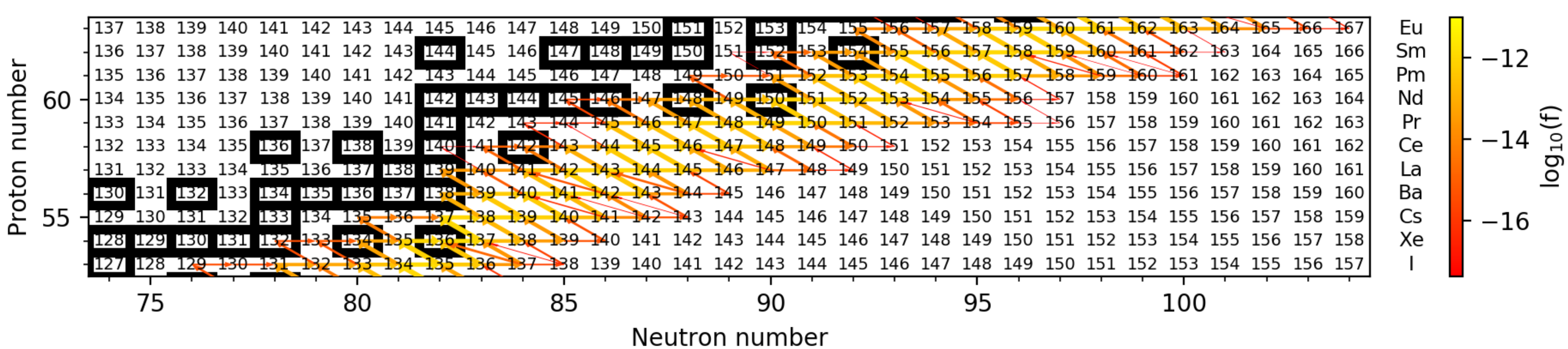

i-process path at N_n=3.16×10^{14} cm^{-3}

Some of the CEMP-*s* stars may actually be the CEMP-*i* stars: multi-zone models

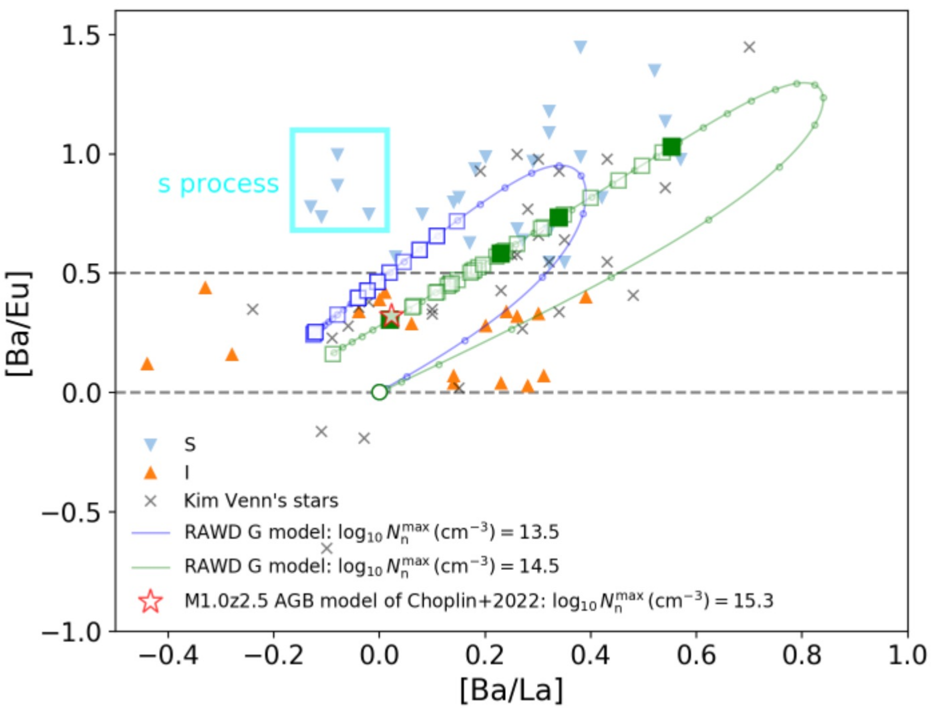

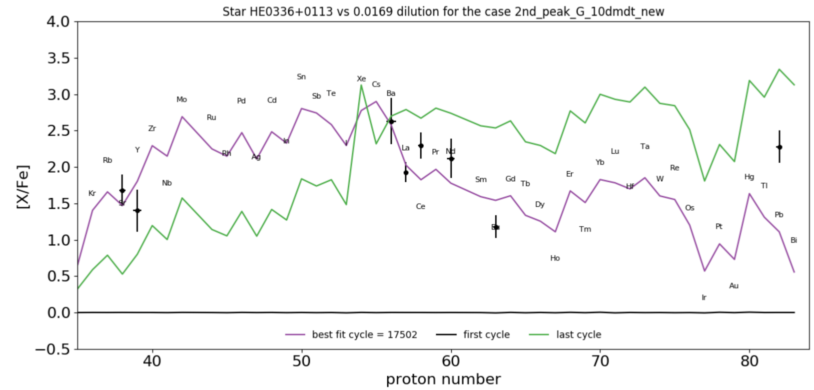

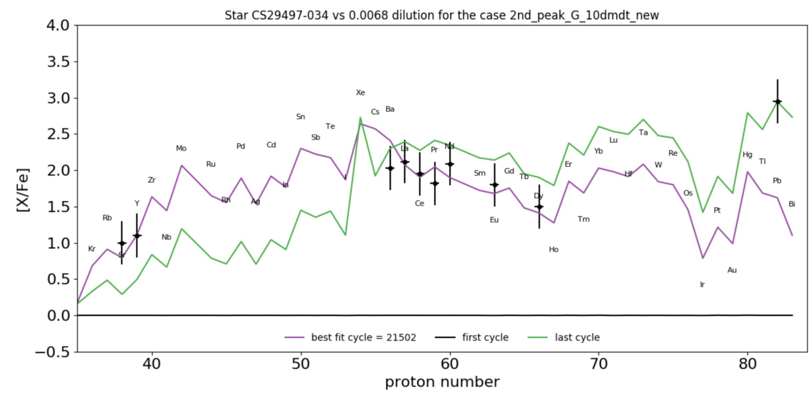

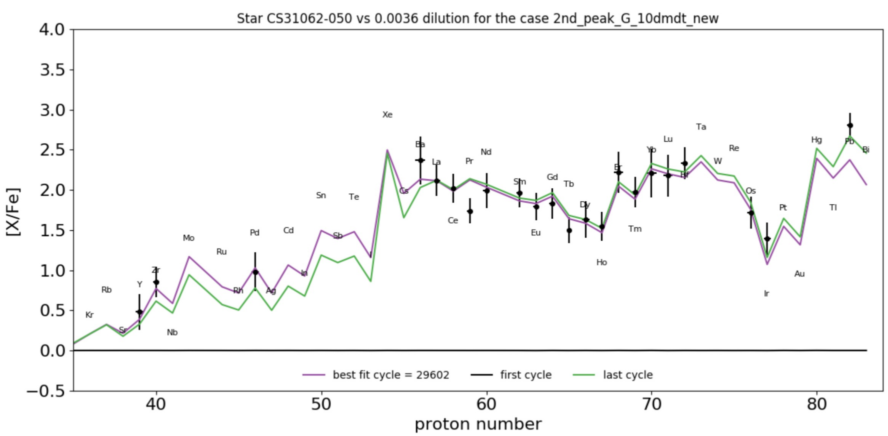

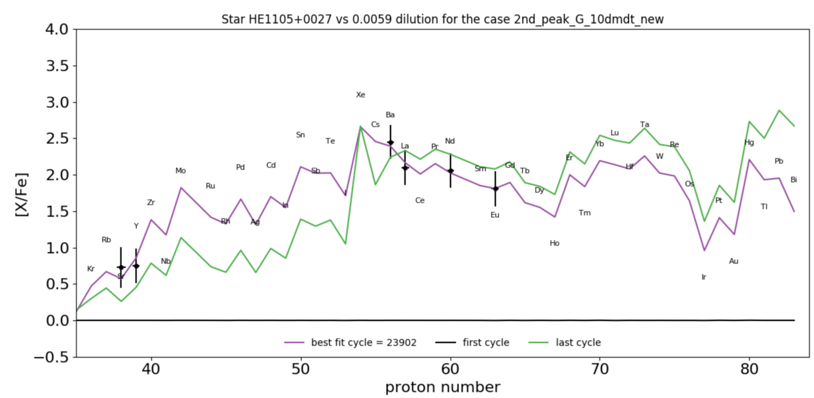

It takes a longer time for [Ba/La] to reach its equilibrium value

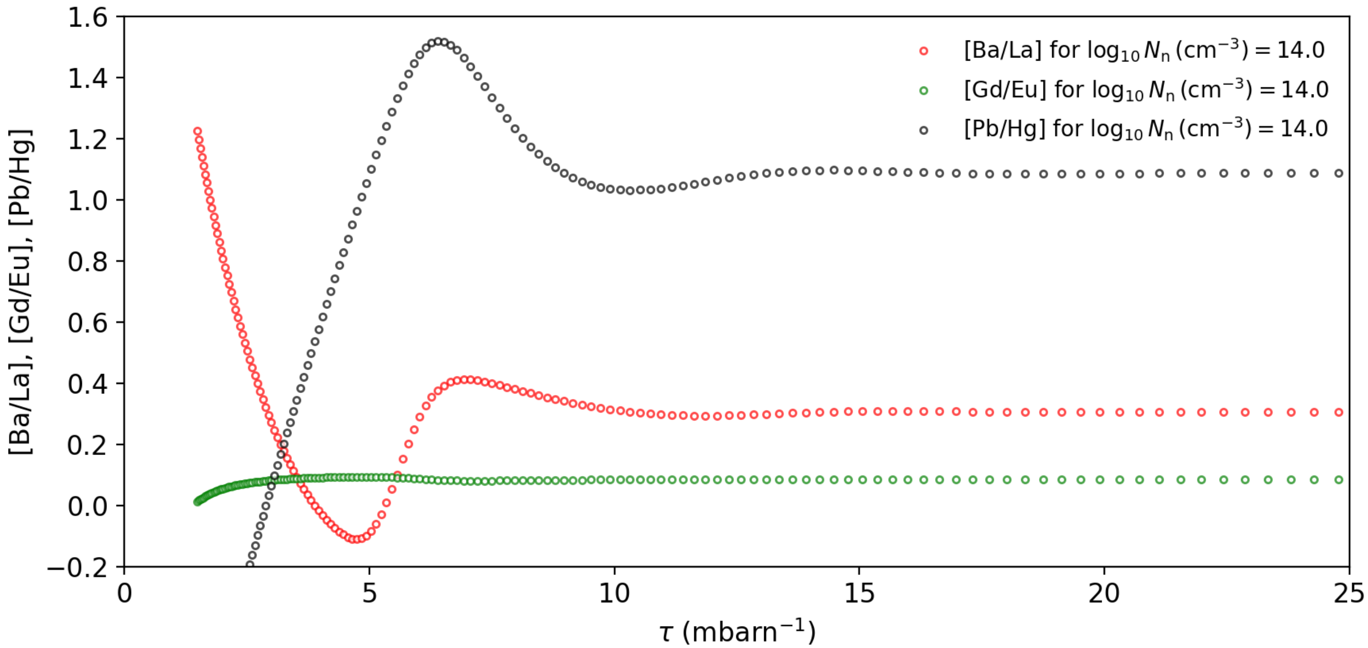

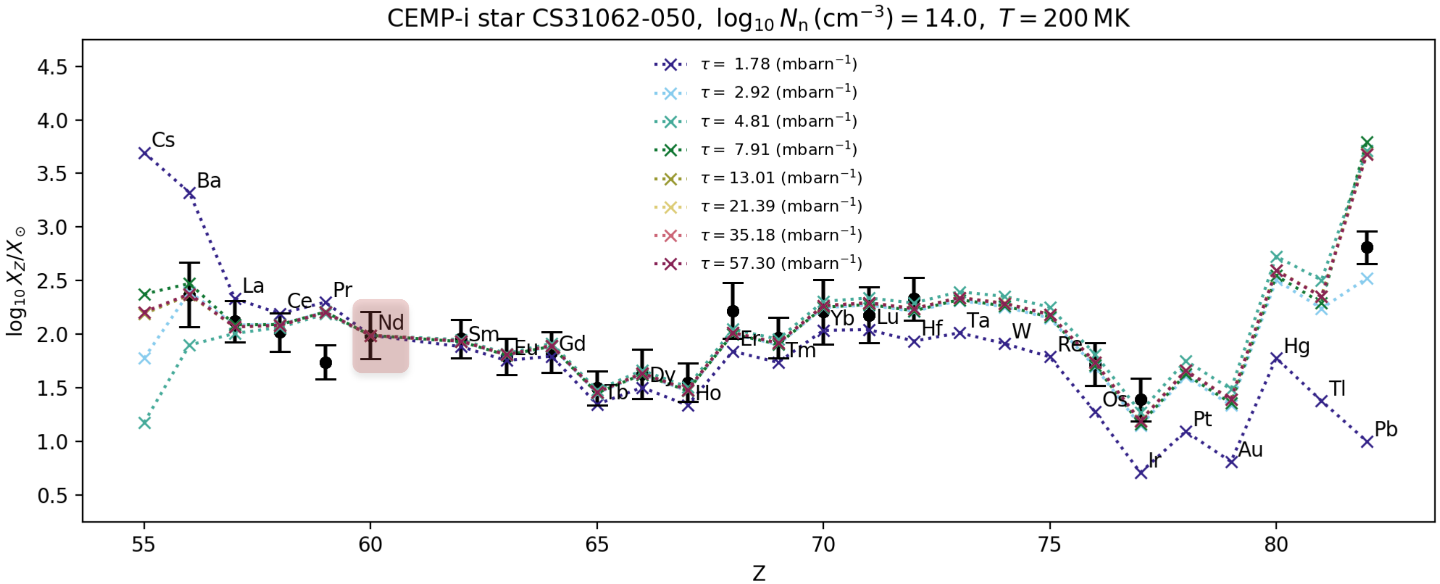

Nd is used as a pin

First, Dardelet, L. et al., (2014nic..confE.145D), and then Hampel, M., et al. (2019, ApJ, 887, 11) estimated $10^{11} \le N_n(\mathrm{cm}^{-3}) \le 10^{14}$ and $1.1 \le \tau\,(\mathrm{mbarn}^{-1}) \le 23.2$ for 24 CEMP-*i*/*r* stars with $N_n = 10^{14}$ cm^{-3} and $\tau = 3.4$ mbarn^{-1} for CS31062-050

Hauser-Feshbach calculations of (n,γ) reaction rates for unstable isotopes

Table 1. List of models used to describe the nuclear level density and the γ strength in the Hauser-Feshbach calculations. Calculations were performed with all 20 possible combinations of these models.

Nuclear Level Density (NLD) models used in this work
Constant Temperature matched to the Fermi Gas (CT+BSFG) (Dilg et al., 1973)
Back-shifted Fermi Gas (BSFG) (Dilg et al., 1973; Gilbert and Cameron, 1965)
Generalized Super fluid (GSM) (Ignatyuk et al., 1979; Ignatyuk et al., 1993)
Hartree Fock using Skyrme force (HFS) (Goriely et al., 2001)
Hartree-Fock-Bogoliubov + combinatorial (HFBS-C) (Goriely et al., 2008)

γ ray Strength Function (γSF) models used in this work
Kopecky-Uhl generalized Lorentzian (KU) (Kopecky and Uhl, 1990)
Hartree-Fock BCS + QRPA (HF-BCS+QRPA) (Goriely and Khan, 2002)
Hartree-Fock-Bogolyubov + QRPA (HFB+QRPA) (Goriely et al., 2004)
Modified Lorentzian (Gor-ML)(Goriely, 1998)

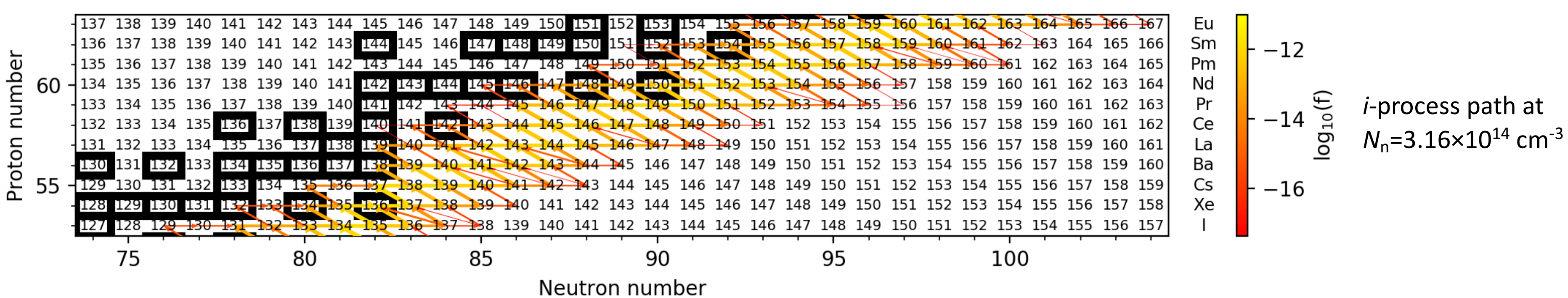

Random variations of (n,γ) reaction rates for unstable isotopes in MC calculations

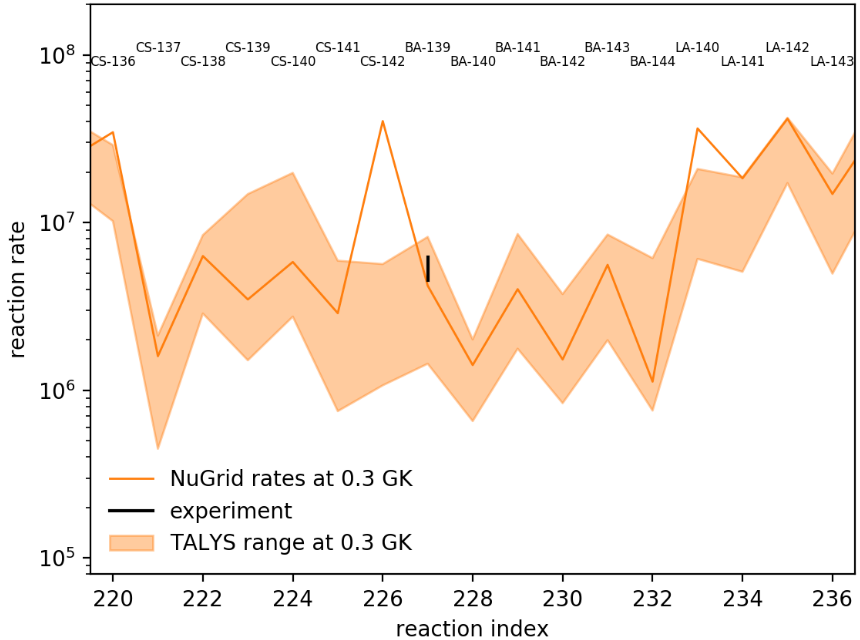

- Experimental (n,γ) rates are used for stable isotopes.
- We ignore possible correlations between (n,γ) rates for selected unstable isotopes (the lower two panels show that when TALYS rates correlate the corresponding experimental rates do not necessarily correlate and can be outside of TALYS ranges, even for stable isotopes).
- We vary (n,γ) rates r_i for selected unstable isotopes multiplying their NuGrid values by the factors $f_i = (p/v_i^{rand}) + (1-p)v_i^{rand}$, where p is assigned a value 0 or 1 with equal probability, and v_i^{rand} are randomly chosen from uniform distributions between 1 and the ratios $v_i^{max} = r_i^{max}/r_i^{min}$ for the TALYS rates.
- This method allows us to identify rates whose variations have the strongest impacts on predicted abundances.

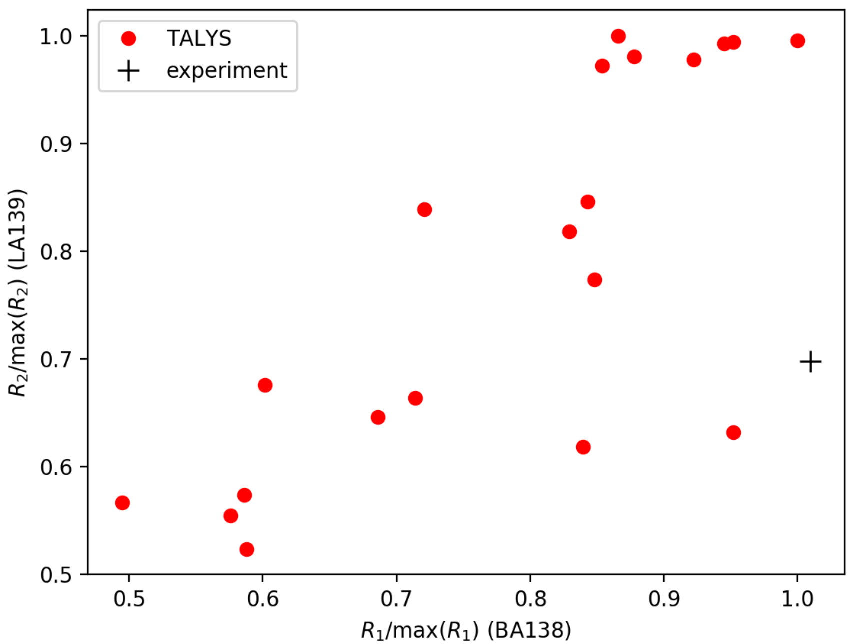

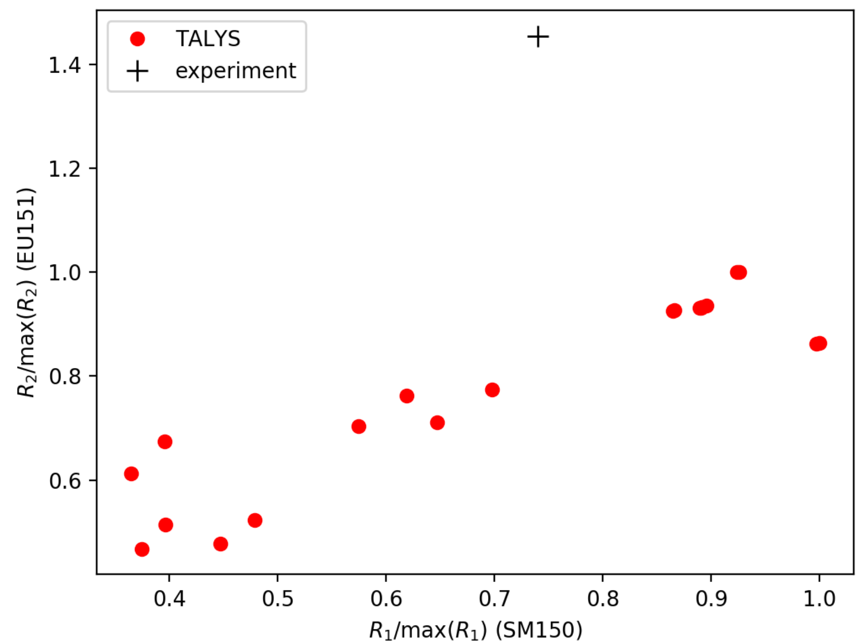

Comparison of MC simulation results for one-zone and multi-zone RAWD models

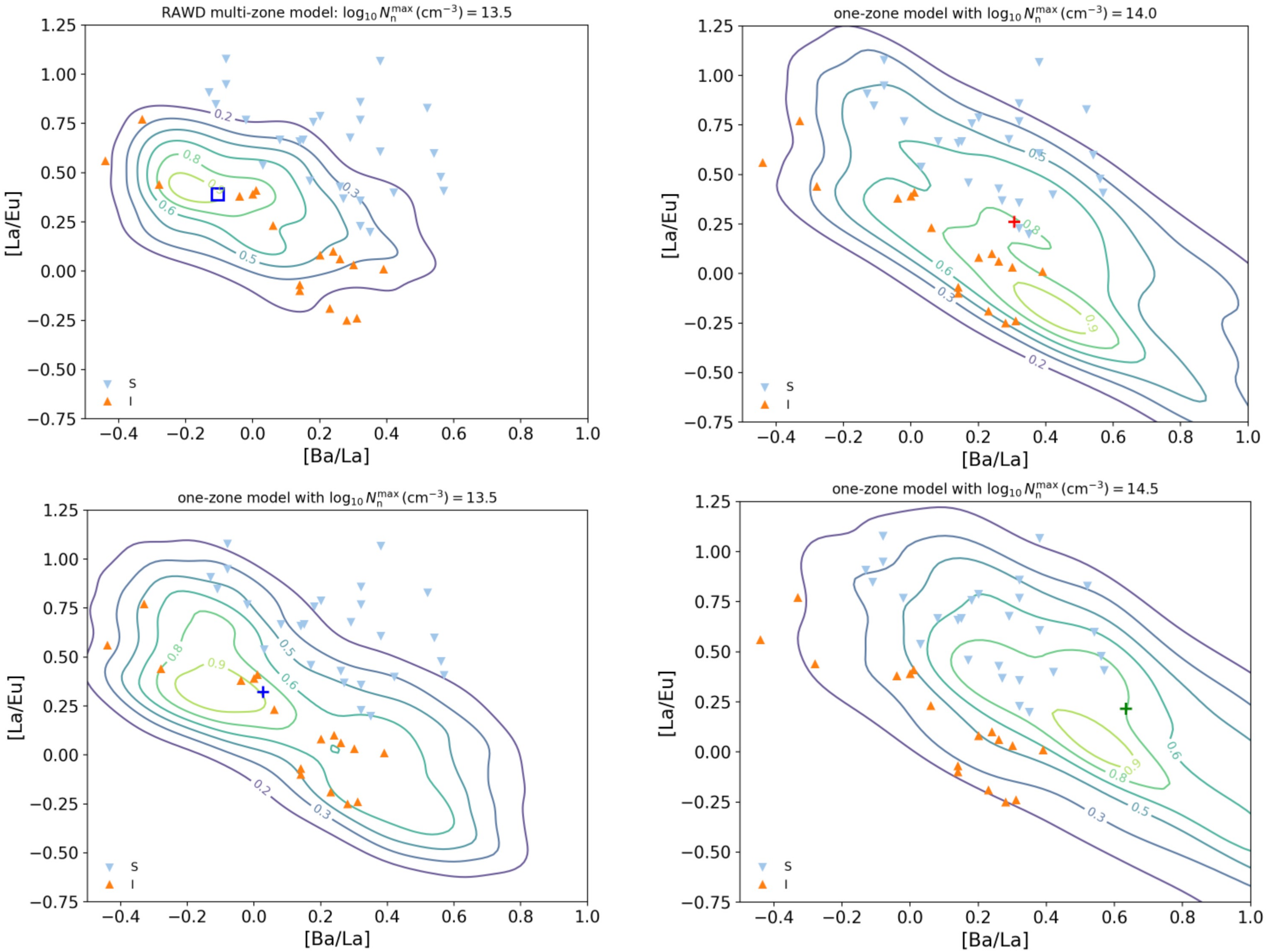

Identifying (n,γ) reaction rates having the strongest impact on the predicted elemental abundance ratios for one-zone model with N_n=3.16×10^{13} cm^{-3}

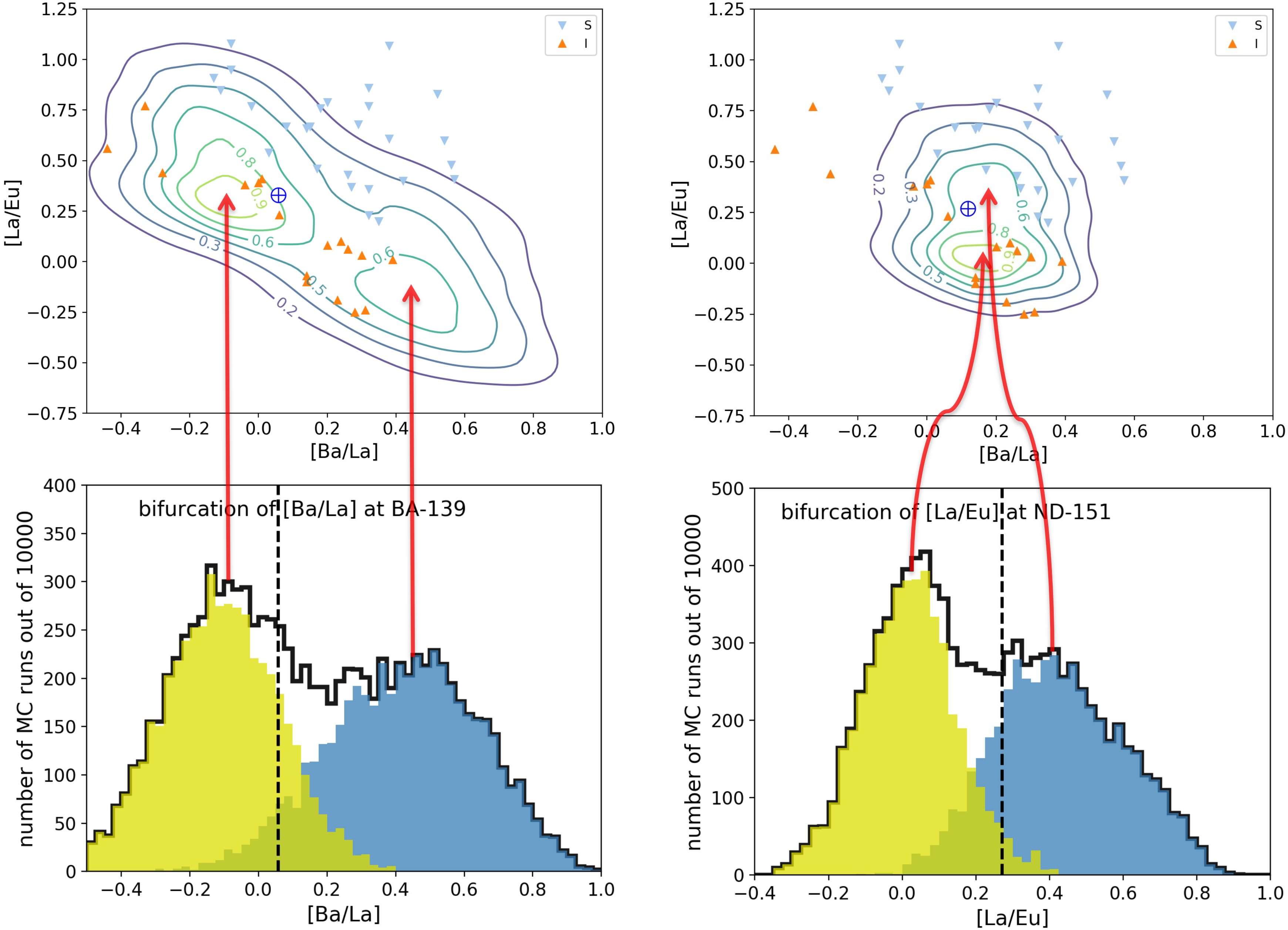

Comparison of MC simulation results for one-zone and multi-zone RAWD models

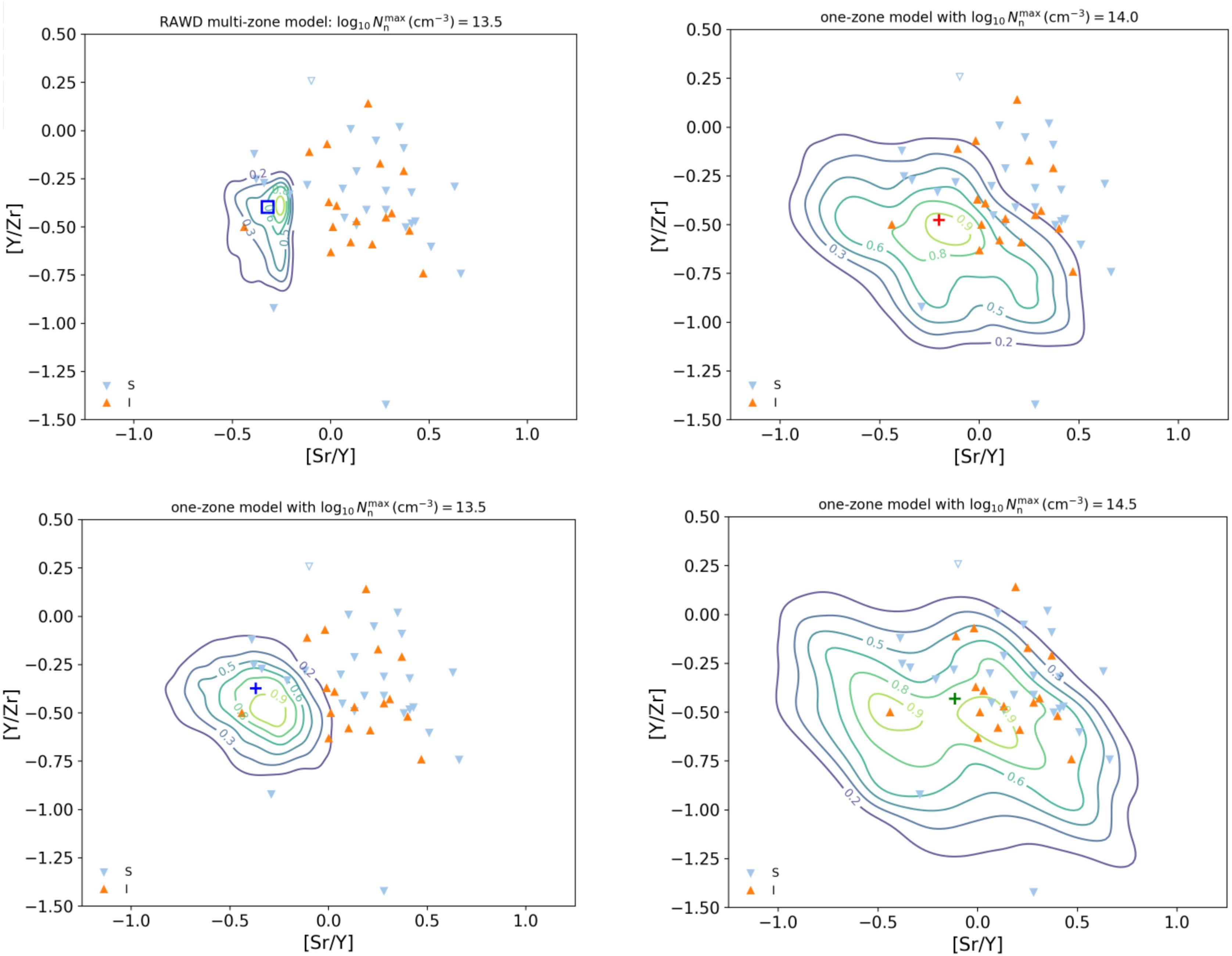

Identifying (n,γ) reaction rates having the strongest impact on the predicted elemental abundance ratios for multi-zone RAWD model

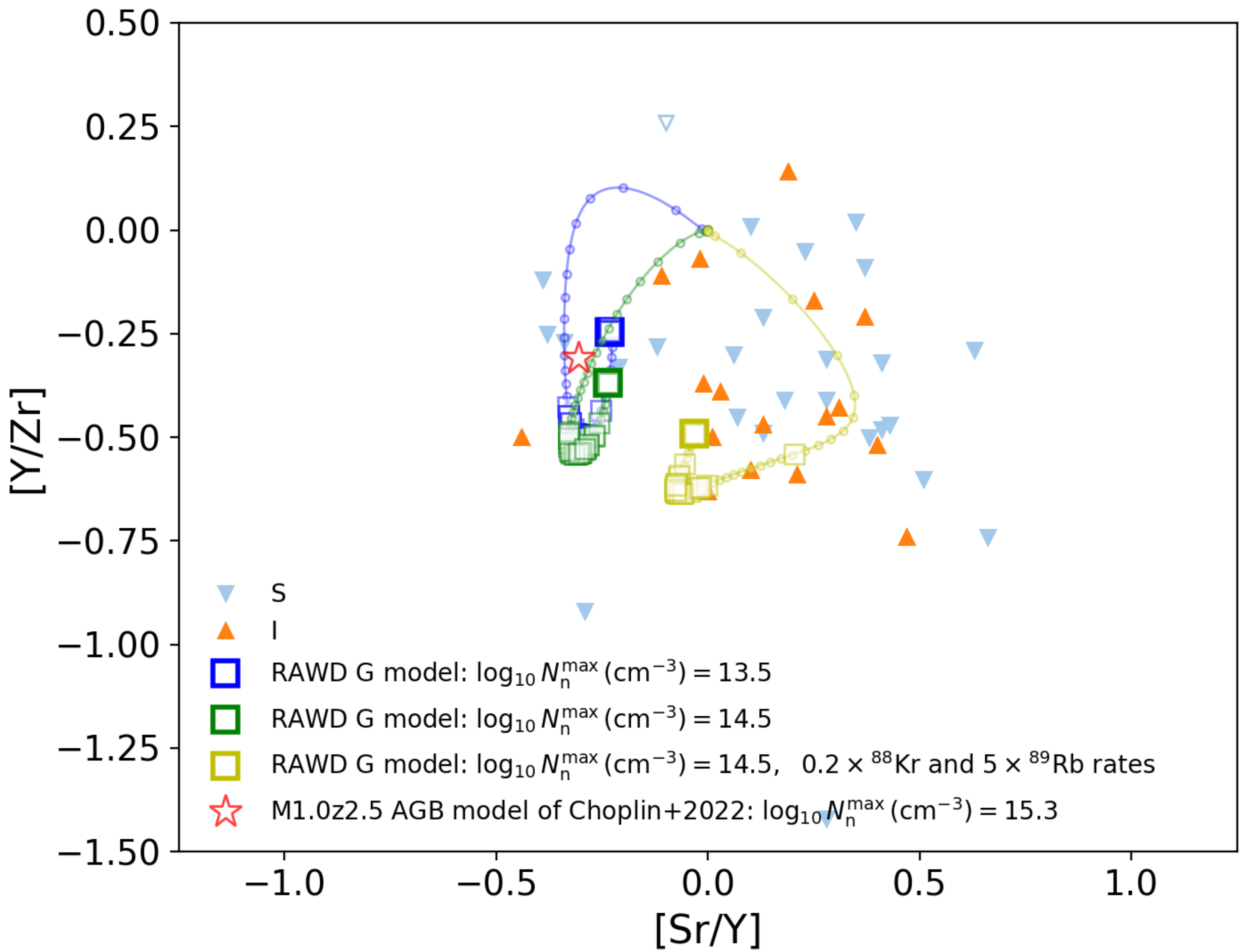

Comparison of *i*-process nucleosynthesis conditions in RAWD and AGB models

From Choplin, A. et al., 2022, A&A, 667, A155

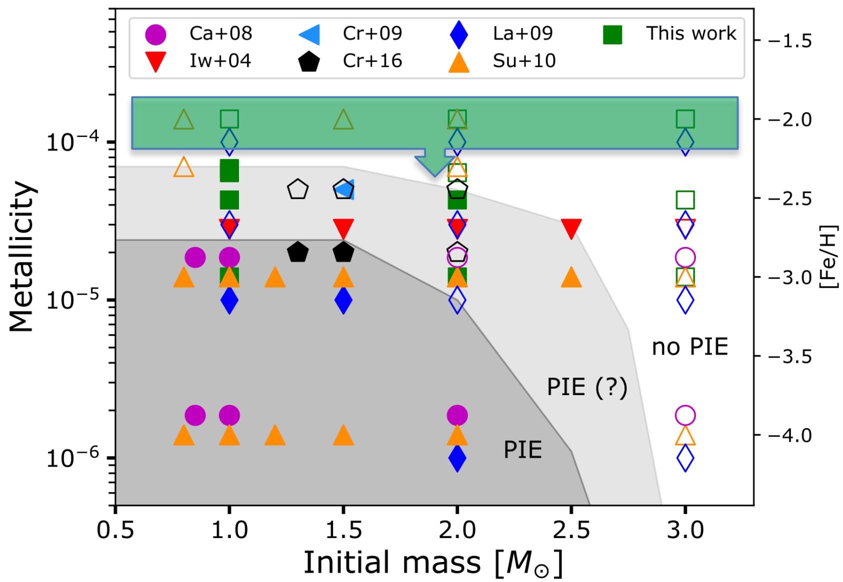

Fig. 3. Mass-metallicity diagram showing the occurrence of PIEs during the early AGB phase of models from various authors. Filled symbols show models experiencing a PIE while empty symbols are for models that do not experience a PIE. The dark grey zone shows the approximate region where PIEs happen in all of the models and the light grey one where PIEs happen in most of the models. The corresponding [Fe/H] ratios are indicated on the right axis assuming solar-scaled mixtures. Models are from Iwamoto et al. (2004, red triangles), Campbell & Lattanzio (2008, magenta circles), Cristallo et al. (2009, blue triangle), Lau et al. (2009, blue diamonds), Suda & Fujimoto (2010, orange triangles), Cristallo et al. (2016, black pentagons). Model results from this work are shown as green squares. All models were computed without extra mixing processes, except the models from Cristallo et al. (2009, 2016), which consider overshooting below the convective envelope.

From Denissenkov, P. et al., 2019, MNRAS, 488, 258

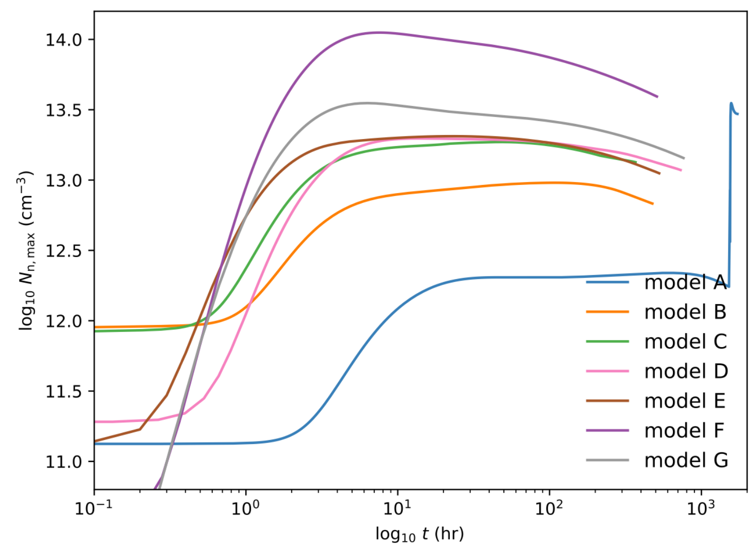

Figure 10. The evolution of the maximum neutron number density in the He convective zones of our RAWD models. In model A, the jump in the evolution of $N_{\rm n,\,max}$ at the end is caused by the switching to the second phase of H ingestion that is shorter but faster than the previous phase (see text).

Table 1. Summary of the one-dimensional RAWD simulation parameters ($L_{\rm He}^{\rm ing}$ is the He luminosity at the beginning of H ingestion).

model	[Fe/H]	$M_{\rm WD}$ ($M_\odot$)	$\dot{M}_{\rm acc}$ ($M_\odot$ yr^{-1})	$\log_{10}(L_{\rm He}^{\rm max}/L_\odot)$	$\log_{10}(L_{\rm He}^{\rm ing}/L_\odot)$	$\dot{M}_{\rm ing}$ ($M_\odot$ s^{-1})	$t_{\rm ing}$ (yr)	η (%)
A	0.0	0.70	2.6×10^{-7}	10.9	9.1	$2.2(35) \times 10^{-12}$	0.17(0.024)	–
B	−0.7	0.71	1.7×10^{-7}	9.5	8.5	2.0×10^{-12}	0.054	4.9
C	−1.1	0.71	1.5×10^{-7}	9.3	8.4	4.0×10^{-12}	0.042	4.9
D	−1.55	0.71	1.5×10^{-7}	9.3	8.5	4.2×10^{-12}	0.083	9.6
E	−2.0	0.74	1.7×10^{-7}	8.7	8.1	3.3×10^{-12}	0.060	27
F	−2.3	0.75	1.5×10^{-7}	9.2	8.6	2.4×10^{-11}	0.058	19
G	−2.6	0.75	1.5×10^{-7}	8.5	8.0	6.7×10^{-12}	0.087	29

Comparison of *i*-process elemental abundances from RAWD and AGB models

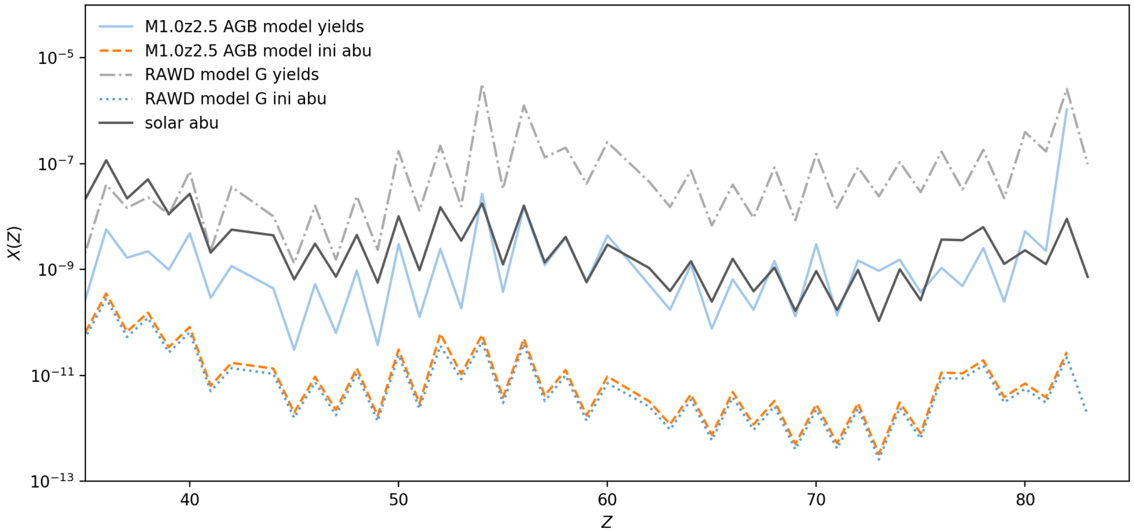

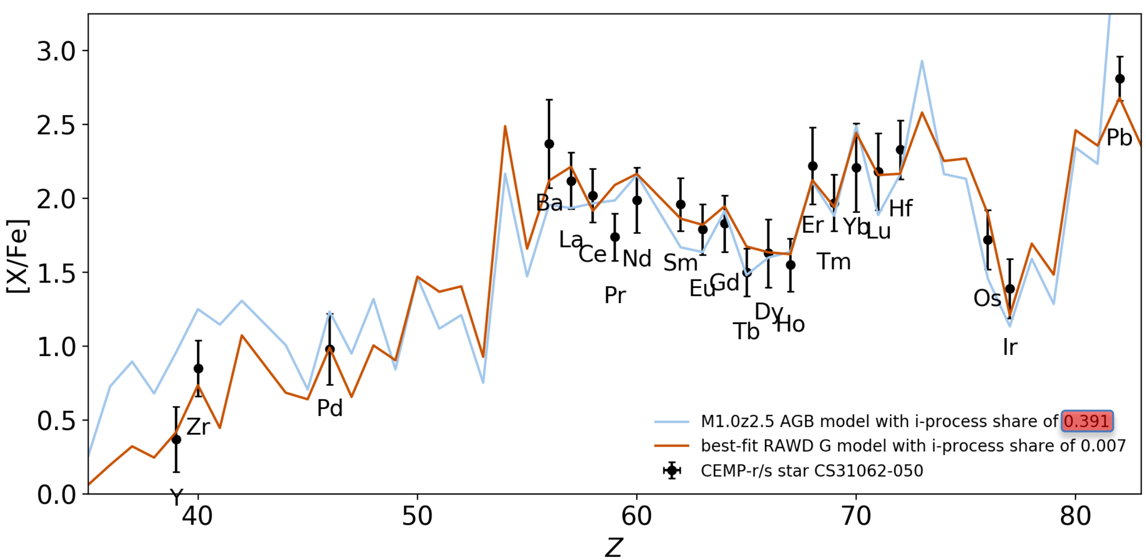

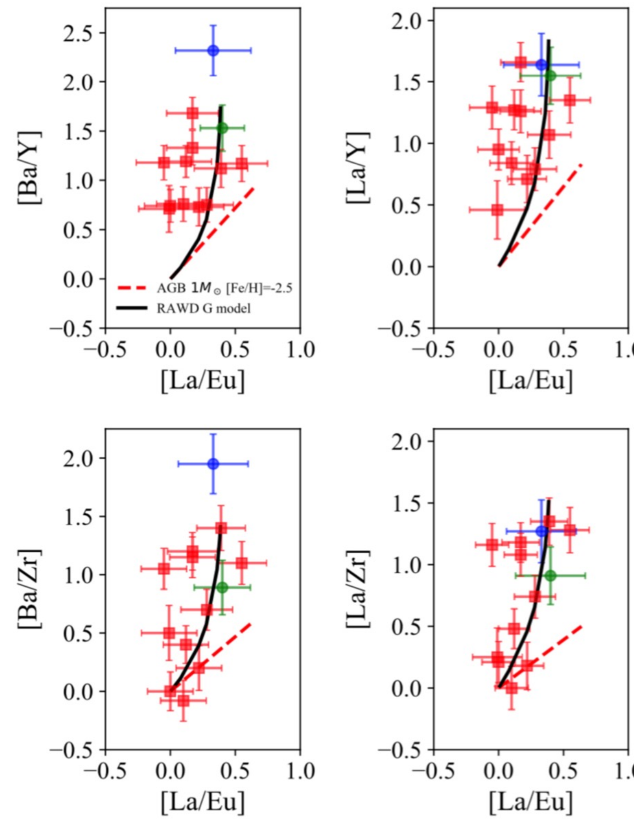

Figure 16. This plot is made to resemble fig. 13 of Karinkuzhi et al. (2021), except that it shows only their CEMP-r/s stars and elemental abundance ratio dilution curve for the 1 $M_\odot$ AGB star model with [Fe/H] = −2.5 (dashed red curves). For a comparison, we have added the stars CS 31062−050 (the blue circle) and HE 2148−1247 (the green circle) and the dilution curve for our RAWD G model (solid black curves).

Comparison of MC simulation results

Table of unstable isotopes whose (n,γ) reaction rate uncertainty has the strongest impact on the predicted *i*-process abundance of a given element (AGB model from Martinet, S. et al. 2024, A&A, 684, A8)

Element	AGB model	RAWD model	$log_{10}N_n$=13.5	
Sr	^{88}Kr	^{88}Rb	^{88}Kr, ^{88}Rb	
Y	^{89}Sr	^{89}Rb	^{89}Rb	
Zr	^{90}Sr	^{90}Sr	^{90}Sr	
Ba	^{137}Xe, ^{137}Cs, ^{138}Cs	^{137}Cs, ^{138}Cs	^{137}Cs	
La	^{139}Ba	^{139}Ba	^{139}Ba	
Ce	^{140}Ba, ^{142}La	^{139}Ba, ^{140}Ba	^{140}Ba	
Pr	^{141}La	^{141}La	^{141}La	
Nd	^{144}Ce	^{144}Ce	^{144}Ce	
Sm	^{147}Pr, ^{147}Nd	^{147}Pr, ^{149}Nd	^{147}Pr	
Eu	^{151}Pm, ^{153}Sm	^{151}Nd, ^{151}Pm	^{151}Nd	
Gd	^{156}Sm	^{156}Sm	^{156}Sm	
Dy	^{161}Tb, ^{162}Tb, ^{163}Tb	^{162}Tb, ^{163}Tb	^{163}Tb	
Er	^{166}Dy	^{166}Dy	^{166}Dy	
Hf	^{177}Yb, ^{178}Yb	^{177}Yb, ^{178}Yb	^{178}Yb	

CaNPAN computational tools and experiments (see at https://canpan.ca)

i-process-tools

Description

This repository (http://206-12-89-164.cloud.computecanada.ca/NuGrid/i-process-tools) contains data files and notebooks that allow to run multiple one-zone simulations of i-process nucleosynthesis for constant neutron densities, analyze results of these simulations and compare them with observational data from the JINAbase and Kim Venn's lists of CEMP-r/s, aka CEMP-i, stars.

Shell scripts, data files and notebooks allowing to prepare and run Monte Carlo simulations for a study of the impact of (n,g) reaction rate uncertainties of unstable isotopes on elemental and isotopic abundances predicted for i process are all in the repository http://206-12-89-164.cloud.computecanada.ca/csa/weak-i-process-impact.

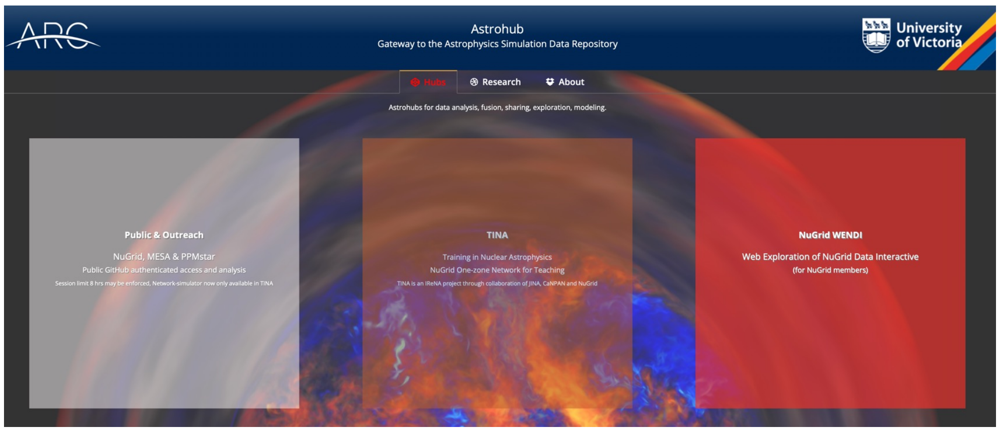

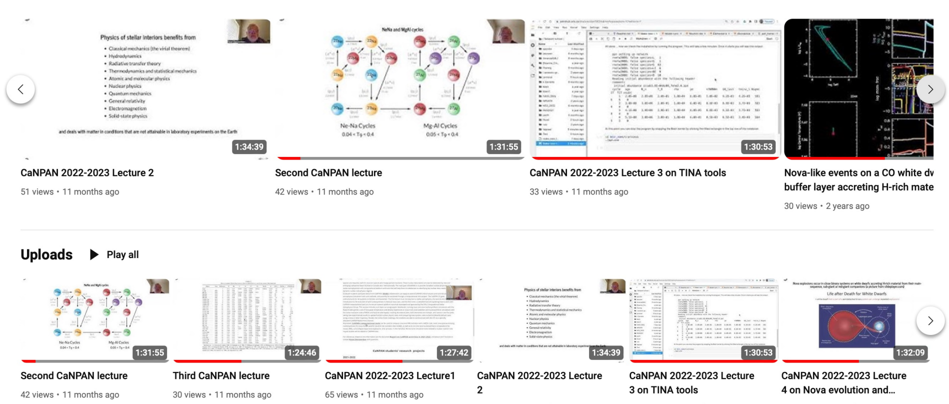

Proposal Number	PI	Title	Species (n,g)
ANL-1734	Ann-Cecilie Larsen	The rare-earth r-process peak: 156-159Sm(n,γ) reaction rates constrained with the beta-Oslo method	155-157Sm
ANL-1742	Artemis Spyrou	Constraints on neutron-capture reactions around N=82	138Ba, 139Ba
ANL-1755	Sean Liddick	Neutron-capture cross section constraints in neutron-rich Sn and Sb isotopes	132Sb, 128-129Sn
ANL-1799	Stephanie Lyons	Constraining neutron-capture cross sections for the i-process	87-89Kr
ANL-1807	Mallory Smith	Investigating gamma-ray strength functions and nuclear level densities in neutron-rich Zr isotopes	96-97Zr, 99Zr
ANL-1812	Adriana Sweet	Neutron-capture cross sections for heavy-mass fission fragments constrained with the β-Oslo method	93-95Sr
ANL-1928	Hannah Berg	Constraining neutron-capture cross section for the i-process around A=150	151-153Nd
ANL-1929 146Ce	Andrea Richard	Neutron-capture constraints for the astrophysical i-process	140Ba, 144Ce,
ANL-2018	Andrea Richard	Constraining i-Process Nucleosynthesis in the Nb-Ru Region	99-101Mo
ANL-2055	Erin Good	Astrophysical i-process constraints via the β-Oslo method	85Kr, 86Br, 92Rb
ANL-e1928 146Ce	Andrea Richard	Neutron-capture constraints for the Astrophysical i-process	140Ba, 144Ce,
ANL-e1929	Hannah Berg	Constraining neutron-capture cross sections for the i-process around A=150	151-153Nd
ANL-e2018	Andrea Richard	Constraining i-Process Nucleosynthesis in the Nb-Ru Region	99-101Mo
FRIB-23084	Steve Pain	Informing the i process: constraining the As/Ge abundance ratio in a metal poor star via 75Ga(d,pg)76Ga	75Ga
FRIB-e23004	Eleanor Ronning	The Last Piece of the Generalized Brink Axel Hypothesis	69Zn, 96Zr
FRIB-e23056	Andrea Richard	Indirect 99Nb(n,g)100Nb Constraint for the Astrophysical i-process	99Nb
	Nicholas Scielzo	Determination of the 92Sr(n,g) cross section and fission product burn up	92Sr
NSCL-e16033	Artemis Spyrou	Study of Kr isotopes for astrophysical applications	85Kr
NSCL-e17014	Sean Liddick	Photon strength function following the decay of 70Cu	70Cu
TRIUMF-S1893	Richard Hughes	Determining the Neutron Capture Cross Section for Unstable 93Sr Via the Surrogate Method	93Sr
TRIUMF-S1944	Denis Mücher	Constraining neutron capture rates for the astrophysical i process	139Ba, 137,139Cs
TRIUMF-S2303	Matthew Williams	Can an i-process explain high [As/Ge] ratios seen in metal-poor stars?	75Ga

CONCLUSIONS

- Most of the CEMP-*r*/*s* stars are actually the CEMP-*i* stars.
- Some of the CEMP-*s* stars may also be the CEMP-*i* stars in which [Ba/La] has not reached its equilibrium value yet, e.g. because of *i*-process shutdown caused by the split of the He convection zone.
- The peak neutron densities characteristic for the *i* process whose signatures are seen in the CEMP-*i* stars lie between 10^{13} and 10^{15} cm^{-3}.
- One-zone models with constant neutron densities can be used in MC computations to identify (n,γ) reaction rates whose uncertainties have the strongest impact on predicted *i*-process elemental and isotopic abundances.
- Right now, the most important reactions whose rates need to be constrained experimentally to improve *i*-process nucleosynthesis models are ^{151}Nd(n,γ), ^{88}Kr(n,γ), and ^{89}Rb(n,γ).
- Unlike RAWD models, the low-mass low-Z AGB models predict lower second- to first-peak elemental abundance ratios than those observed in the CEMP-*i* stars, require too high fractions of *i*-process abundances in them, and they seem to disagree with the lack of CEMP-*i* stars in globular clusters with [Fe/H] $\lesssim$ -2 and signatures of *i*-process nucleosynthesis in pre-solar dust grains (see my talk tomorrow).